LBL-31057

Center for Advanced Materials

CAM

Theory of Ordering Transformations in Metals and Minerals

T.F. Lindsey
(Ph.D. Thesis)

July 1991

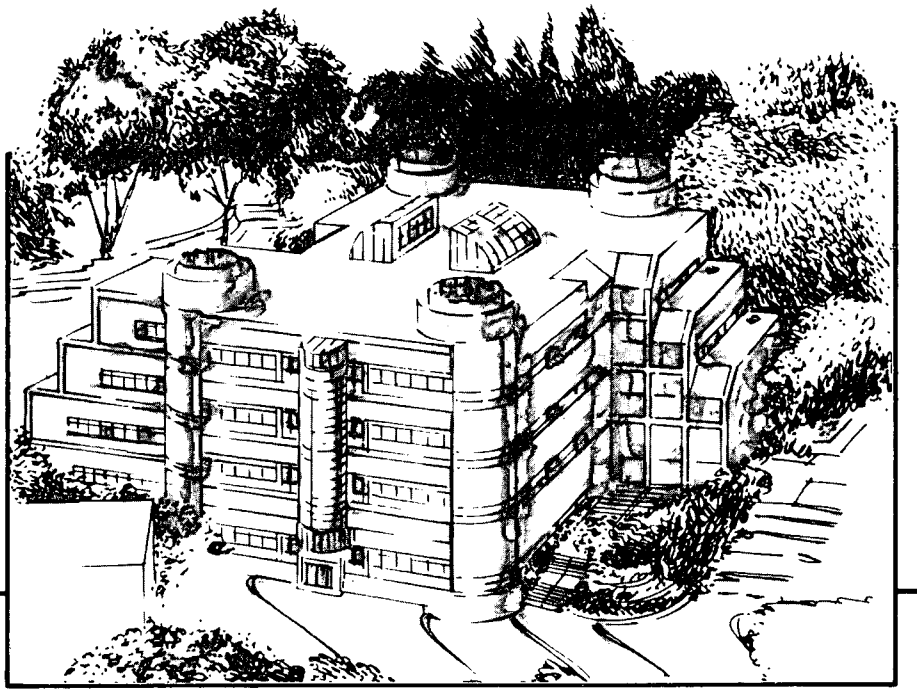

Materials and Chemical Sciences Division

Lawrence Berkeley Laboratory • University of California

ONE CYCLOTRON ROAD, BERKELEY, CA 94720 • (415) 486-4755

Prepared for the U.S. Department of Energy under Contract DE-AC03-76SF00098

LOAN COPY
Circulates
for 4 weeks
Bldg. 50 Library.
LBL-31057
Copy 2

DISCLAIMER

This document was prepared as an account of work sponsored by the United States Government. While this document is believed to contain correct information, neither the United States Government nor any agency thereof, nor the Regents of the University of California, nor any of their employees, makes any warranty, express or implied, or assumes any legal responsibility for the accuracy, completeness, or usefulness of any information, apparatus, product, or process disclosed, or represents that its use would not infringe privately owned rights. Reference herein to any specific commercial product, process, or service by its trade name, trademark, manufacturer, or otherwise, does not necessarily constitute or imply its endorsement, recommendation, or favoring by the United States Government or any agency thereof, or the Regents of the University of California. The views and opinions of authors expressed herein do not necessarily state or reflect those of the United States Government or any agency thereof or the Regents of the University of California.

LBL 31057

Theory of Ordering Transformations in Metals and Minerals

Timothy Francis Lindsey

Ph.D. Dissertation

Department of Materials Science and Mineral Engineering
University of California
and
Center for Advanced Materials
Materials Sciences Division
Lawrence Berkeley Laboratory
University of California
Berkeley, CA 94720

July 1991

This work was supported by the Director, Office of Energy Research, Office of Basic Energy Science, Materials Science Division of the U.S. Department of Energy under Contract No. DE-AC03-76F00098

Theory of Ordering in Metals and Minerals

by

Timothy Francis Lindsey

ABSTACT

This dissertation presents an investigation of ordering in FCC based systems using the pair potential approximation in the ground state and mean field limits. The theoretical approach is used to explain the occurrence of observed equilibrium phases and characteristics of thermodynamic instabilities, in particular, spinodal ordering and decomposition.

It is shown that the stability of non-integer domain sizes in long period superstructures such as Al_3Ti and Ag_3Mg may result from the tendency of a system to reduce the number of non-dominant ordering waves, thus producing domain sizes that have the rational fraction form n/m. This conclusion is used to explain the domain size stability with respect to variations in temperature and electron concentration.

The cation ordering in the precipitate phases in calcite and dolomite is analyzed by analogy with ordering in FCC based metals. The ordered phases in calcite and dolomite are shown to be consistent with pair potential minima at $\{100\}$ and $\{\frac{1}{2}, \frac{1}{2}, \frac{1}{2}\}$ positions in reciprocal space respectively. The results of the thermodynamic analysis show that the ordered phases may have resulted from an ordering instability of the disordered matrix. This suggests that the ordered precipitates form spontaneously on the surface of

TABLE OF CONTENTS

1. INTRODUCTION

I. Background 1

II. Mean-Field Limit 3

III. Value of Phenomenological Models 5

IV. Applications for FCC Based Systems 7

2. STABILITY OF NON-INTEGER DOMAIN SIZE IN LONG PERIOD SUPERSTRUCTURES

I. Introduction 10

II. Theory 14

III. Discussion and Conclusions 22

Figures for chapter 2 32

3. CATION ORDERING IN CALCITE AND DOLOMITE

I. Introduction 44

II. Theory 49

III. Discussion and Conclusions 60

Tables for chapter 3 65

Figures for chapter 3 67

4. PRECIPITATION OF $L1_2$ PHASE IN FCC BASED ALLOYS

I. Introduction 70

II. Transformation Paths and Mechanisms 73

III. Thermodynamics 76

IV. Application to δ' precipitation in $Al - Li$ 87

V. Discussion and Conclusions 94

Figures for chapter 4 96

5. SUMMARY 102

6. REFERENCES 105

ACKNOWLEDGEMENTS

I would like begin by thanking my research advisor, J. W. Morris, Jr, for his encouragement, patience, understanding, and inspiration during my long years of graduate study. My association with him has been a great pleasure and privilege. I will always be grateful for his sincere and genuine interest in my welfare as a graduate student and as a person.

It has been my good fortune to work with Professor R. Wenk. He has opened my eyes to new fields of theoretical inquiry and has been an enthusiastic supporter of my research interests. Working in collaboration with him has been a great pleasure.

I am thankful to Professor R. Gronsky for his words of encouragement and advise to me. His interest in my research has been an inspiration to me. My interactions with him have been a pleasurable experience.

I cannot thank enough my dear friend, Marta Munoz, who has been an invaluable source of encouragement throughout my graduate study.

As I work towards the completion of my Ph.D. degree, it is with special thanks that I recognize my parents for all that they have done for me. Their moral support and unwavering belief in my ability has propelled me forward over many difficult obstacles.

This work was supported by the Director, Office of Basic Science, U.S. Department of Energy under contract No. DE-AC030-76SF0098.

CHAPTER 1

INTRODUCTION

I. Background

The problem of predicting the ordering transition temperature for alloys is an important theoretical problem. The simplest technique of estimating the transition temperature is the Braggs-William mean-field method [1]. While this method gives a good qualitative explanation of the emergence of the long-range order parameter [2-3], it does not accurately predict the transition temperature [4]. Bethe [5] and Peierls [6] showed that better agreement with experiment results can be obtained by taking the near-neighbor correlations into account using statistical mechanics. Their approach considered the thermodynamics of a cluster which experiences the average potential due to the surrounding atoms. Kikuchi developed a method of determining the entropy of system with a specified set of cluster probability values [7]. This method has been extensively used to calculate phase diagrams and is presently known as the cluster variational method [4].

The cluster variational method provides a means of both determining the free energy and the short-range order parameters. Another method that may be used to calculate the free energy is the Kirkwood method [8]. This method assumes near neighbor interactions. However, as shown by Badalyan and Khachaturayan, the Kirkwood method can be generalized for the case of arbitrary range pair interactions [9]. The Kirkwood method gives the free energy as expansion in powers of inverse temperature for a given composition

and long-range order parameter(s). While the short-range order parameters do not explicitly appear in the Kirkwood free energy series, the effect of the short-range correlations is taken into account via computation of the cummulant energy moments.

When the predictions of the mean-field method and the more accurate cluster variation method are compared, the mean-field estimation of the transition temperature is found to be highly inaccurate [4]. For example, it may be shown that the maximum mean-field transition temperature for the Cu_3Au phase is at composition 0.50. However, by taking correlations into account using the cluster variational method, the maximum transition temperature for Cu_3Au phase is at the stoichiometric composition 0.25 Au [4].

Although the mean-field approximation is highly inaccurate at temperatures near the transition point, at temperature well above or below the transition point, the mean-field method is a good approximation [10]. This is a very important result because materials are often processed at temperatures that are sufficiently low for the mean-field to be a good approximation [11]. When this is the case, it is not necessary to use the more accurate, but also more complicated, statistical mechanical methods such as the cluster variation method or Kirkwood expansion.

The recognition that the mean-field method is a good approximation at low temperature is important because it is very simple and requires little computational effort. In this thesis, the theoretical analysis will use ground

state and mean-field analysis. The justification of this approach is that the ordering phenomena that will be discussed occurs at sufficiently low temperatures to justify the use of mean-field or ground state theory. However, since the inaccuracy of the mean-field method at higher temperatures is very well known [4], I will now provide an explanation of why the mean-field approximation is valid at sufficiently low temperatures.

II. The Mean-Field Limit

The free energy may be expanded in powers of inverse temperature using the thermodynamic perturbation series [12],

$$F = F^0 + M_c^1 - \frac{1}{2T} M_c^2 + \cdots \tag{2.1}$$

where F_0 is the unperturbed free energy and M_c^n are the nth order cummulant moments [13] of the perturbation energy distribution,

$$M_c^1 = < \delta E > \tag{2.2a}$$

$$M_c^2 = \left\langle (\delta E - < \delta E >)^2 \right\rangle . \tag{2.2b}$$

The notation $< \cdots >$ refers to the ensemble average of the quantity $(\cdots)$ and δE is the perturbation energy. If the perturbation energy is chosen such that $< \delta E >$ is zero, then equation (2.1) takes the form

$$F = F^0 - \frac{1}{2T} < (\delta E)^2 > + \cdots \tag{2.3}$$

where F^0 is the mean-field free energy. Badalyan and Khachaturyan evaluated equation (2.3) assuming that the configurational energy is given by the pair potential formula,

$$E = \frac{1}{2} \sum_{rr'} V_{r-r'} n_r n_{r'} , \tag{2.4}$$

where V_r is the interaction pair potential and n_r is the solute distribution function. It has value 1 if site r is occupied by a solute atom and zero otherwise. Taking the unperturbed energy to be

$$E^0 = \frac{1}{2}\sum_{rr'} V_{r-r'} p_r p_{r'}, \tag{2.5a}$$

where p_r is the ensemble average of the solute occupation at site r, i.e., $p_r =< n_r >$, and the perturbed energy to be

$$\delta E = \frac{1}{2}\sum_{rr'} V_{r-r'} \delta n_r \delta n_{r'}, \tag{2.5b}$$

where δn_r is defined by the relation

$$\delta n_r = n_r - p_r, \tag{2.5c}$$

Badalyan and Khachaturyan showed that F_0 is the mean-field free energy,

$$F^0 = E^0 - TS^0, \tag{2.6a}$$

$$S_0 = -\sum_r \left(p_r \ln p_r + (1-p_r)\ln(1-p_r)\right), \tag{2.6b}$$

and that leading term in perturbation series is

$$\delta F^1 = -\frac{1}{2T}\sum_{rr'} V^2(r-r') p_r(1-p_r)\, p_{r'}(1-p_{r'}). \tag{2.6c}$$

As the temperature is decreased, the solute occupation probability value p_r at each site r tends to either the value 1 or 0. In either case, the product $p_r(1-p_r)$ tends towards zero as the system approaches the ground state. It can be shown that the limit $T \to 0$, the term

$$\frac{1}{T} p_r(1-p_r)\, p_{r'}(1-p_{r'}) \tag{2.7}$$

tends to zero. Hence, in the low temperature limit, the first correction to the free energy tends to zero, and in the ground state limit the first correction vanishes. Therefore, at sufficiently low temperature the free energy is given accurately by the mean-field formula. This is the result also obtained by Krivoglaz who considered the thermodynamics of nearly ordered crystals. [10].

In the ground state limit, the mean-field entropy S_0 tends to zero. This result follows from equation (2.6b), since it may be shown that the limit as x goes to zero or one, the quantity

$$x \ln x + (1 - x) \ln(1 - x)$$

tends to zero. Hence, for systems that are very nearly fully ordered, the free energy is accurately given by the mean-field energy E^0.

III. Value of Phenomenological Models

It is often useful to discuss ordering phenomena within the context of a phenomenological model because this permits the ordering in different types of crystals to be discussed using a common theoretical prospective. The value of this approach is that it allows one to explain the general characteristics of a material in a simple way. For example, the competition between volume and surface energy provides a simple means of explaining the concept of a critical nucleus. However, to predict the actual critical nucleus size from first principles would be very complicated. This would require an estimation of the bonding forces and a statistical mechanical calculation of free energy. The degree of accuracy that is built in the calculation depends

on one's objectives. If one wishes to start with atomic numbers and derive results that reproduce experimental observations, then a high degree of accuracy will be required. However, if one only seeks to explain the main idea, a simple theory that is not necessarily very accurate may be sufficient. For instance, the Braggs-William theory does not accurately predict the transition temperature, but does correctly explain ordering transformations at the conceptual.

Compared with the more accurate methods such as the cluster variational method [4,7] and free energy expansion methods [8,9], the mean-field and ground state methods of analysis may seem less useful. However, on the contrary, these simpler methods may give better conceptual insight. For this reason, simple theories still have considerable value and continue to be widely used in the theoretical investigations of materials.

The use of the pair potential model is phenomenological in situations where the pair potential function is regarded as an adjustable parameter. Even without knowledge of what the actual pair potential function is for a given system of interest, the results of the general pair potential can be discussed after making some physical assumptions. For example, the range of the pair potential function may be assumed to extend to only first and second near-neighbors. The two simplest levels of approximation to calculate the free energy of a system where the atoms interact in pairs are the ground state and mean-field methods. While the mean-field method is not accurate at temperatures near the transition point, it is a good approximation at temperatures well below the transition point. The value of using the ground

state and mean-field method together with the pair potential approximation is that this provides the simplest means of explaining and understanding low temperature thermodynamic behavior.

IV. Applications For FCC Based Systems

In this thesis, the ground state and mean-field method of analysis will be used to investigate three selected examples of FCC based ordering transformations. This type ordering occurs when the ordering species are distributed over the sites of a face centered cubic (FCC) array. These examples were chosen because they illustrate how the low temperature thermodynamic behavior may be explained in a simple way using the pair potential approximation.

The pair potential may be defined in either real space or reciprocal space. Since ordered phases are a superposition of ordering waves, it is useful to use the reciprocal space representation of the pair potential. This quantity is obtained from the real space pair potential $V(r)$ by using the definition of a Fourier transform,

$$V(k) = \sum_{r} V(r)\, e^{i2\pi k\cdot r}. \tag{4.1}$$

However, since the pair potential will be regarded as a phenomenological quantity, the values of $V(k)$ will be treated as adjustable parameters.

Whereas the real space function $V(r)$ may have an infinity of values corresponding to the infinity of ordering sites of the crystal, only a finite number of $V(k)$ values determine the mean-field free energy. This is expected

since an ordered phase is a superposition of a finite number of ordering waves. Moreover, $V(k)$ will have the same value for wave vectors that are related by the symmetry of the fundamental lattice. Hence, the number of independent pair potential parameters that determine the mean-field free energy may be very small. For example, it may be shown that for Cu_3Au, there are just two independent pair potential parameters.

The reciprocal space positions corresponding to the minima of the pair potential function $V(k)$ have a significant effect on the thermodynamic properties of ordered phases. This result has been discussed by Clapp and Moss [14]. They presented experimental evidence showing that the ordering wave vectors are determined by $V(k)$ minima positions, and explained their findings by a consideration of the ground state energy minimization problem. Moreover, Khachaturyan [11] has shown that in the mean-field limit, the high temperature ordering instability is due the formation of ordering waves with wave vectors corresponding to the $V(k)$ minima. The ordering wave vectors are not always determined by the $V(k)$ minima positions, since a specified composition, it is not always possible to construct a ground state phase containing ordering wave vectors from the star of k corresponding to the $V(k)$ minima [13]. Nevertheless, it is often the case that the ordering wave vectors are determined by the positions the $V(k)$ minima [14].

In the theoretical treatment presented in this thesis, the relationship between the $V(k)$ minima positions and the equilibrium ordered state will be a central theme. Chapter 2 presents a ground state investigation of long-period superstructures. It is shown that the maximum amplitude or-

dering wave vector is approximately determined by minimum position of $V(k)$ along the reciprocal space line joining $(1,0,0)$ and $(1,0,1)$. Chapter 3 presents a ground state and mean-field analysis of the cation ordering of ordered precipitate phases that are observed in calcite and dolomite. It is shown that the experimental observations are consistent with the existence of pair potential minima at the special point positions $\{1,0,0\}$ and $\{\frac{1}{2},\frac{1}{2},\frac{1}{2}\}$. Chapter 4 presents a mean-field calculation of the $Al-Li$ phase diagram and instability limits at low temperatures. The theoretical method assumes that the $V(k)$ minima for $Al-Li$ are at the special point positions $\{1,0,0\}$. This assumption is shown to provide a good explanation of the conditions for spinodal ordering and decomposition in the $Al-Li$ alloy system.

CHAPTER 2

STABILITY OF NON-INTEGER DOMAIN SIZE IN LONG PERIOD SUPERSTRUCTURES

This chapter presents a theoretical investigation of the equilibrium conditions for long period superstructure ordering. Assuming pairwise interactions, the stability of rational fraction domain sizes and Fujiwara's assumption of square wave modulation of domain boundaries is predicted by the minimization of the configurational energy. The results of the pair potential theory are interpreted using Khachaturayan's concept of dominant and non-dominant ordering waves. While the domain size M is determined by the wave vector of the dominant ordering wave, the stability of non-integer periods are shown to result from the influence of the non-dominant ordering waves. The variation of domain size with valence electron concentration and temperature is discussed.

I. INTRODUCTION

A well known example of long period ordering is $CuAu(II)$ [16]. This structure results from a periodic sequence of displacements of a $L1_0$ cell as shown in figure 1(a). Sato and Toth showed that the experimentally observed relationship between the valance electron to atom ratio (e/a) and the domain size M agrees well with the formula

$$\frac{e}{a} = \frac{\pi}{12t^3}(2 \pm \frac{1}{M} + \frac{1}{4M^2})^{3/2} \tag{1.1}$$

which was derived from a band theory argument [16]. The Sato-Toth theory, using the idea of long period ordering caused by a fermi-level effect, explains the $AuCu(II)$ type LPS very well, and thus it has become widely accepted [17].

In alloys such as Ag_3Mg [18] and Al_3Ti [19], a different type of LPS is observed. These are produced by a periodic sequence of displacements of a $L1_2$ cell as illustrated in figure 1(b). In a survey of long period structures of this type, Schubert [20] showed that the domain size M is related to the valence electron concentration by the empirical formula

$$\frac{1}{2M} \approx (e/a) - 1. \tag{1.2}$$

He also showed that the axial ratio c/a of the fundamental cell is likewise linearly related to the valence electron concentration.

The domain size M is defined by the Fujiwara square wave function [21]. This function is generated by a square wave with half period M and sampled over discrete points, i.e.,

$$f(n) = \begin{cases} +1 & \text{if } \cos(\frac{\pi}{M}n) > 0 \ , \\ 0 & \text{if } \cos(\frac{\pi}{M}n) < 0 \ . \end{cases} \tag{1.3}$$

where the value of $f(n)$ indicates whether or not the nth cell is shifted by the displacement vector $\frac{1}{2}(110)$. The function $f(n)$ is $+1$ for a unshifted cell and 0 for shifted cell at position n.

Equations (1.1) and (1.2) suggest that the domain size varies continuously with the valence electron concentration. However, for the Ag_3Mg and Al_3Ti alloys, M values are observed to be of the irreducible fraction form

$M = (s/L)$. These long period superstructures may have a fixed domain size over a range of both temperature and composition.

Tachiki and Maekawa [22] investigated stability of the domain size against small variations in the valence electron concentration by calculating the configurational energy assuming that the interaction pair potential function has the Lorentzian form

$$V(0,1,k_z) = \frac{-\alpha}{1 + (\frac{k_z - k_z^{min}}{\Delta})^2} \tag{1.4}$$

along the reciprocal space line joining (010) and $(01\frac{1}{2})$. Using equation (1.4), they determined the domain size that minimizes the configurational energy. Their results show that the domain size decreases in steps as the minimum position k_z^{min} is varied. The width of these steps decreases as Δ increases. This lead Tachiki and Maekawa to conclude that the domain size will deviate slightly from the relation $2M = 1/k_z^{min}$ that would be obtained if the domain size were assumed to correspond to the minimum of equation (1.4).

Tachiki and Teramoto [23] calculated the band structure for the $Cu-Au$ system as a function of the electron concentration (e/a). They observed that the electron eigen energies for the unperturbed Hamiltonian H_0 had the general shape of a Lorentzian function. The variation in the minimum position of $H_0(0,1,k_z)$ with (e/a) was approximately linear. Hence, they assumed that parameter k_z^{min} of the Lorentzian function in equation (1.4) varies with the electron concentration according to the relation $k_z^{min} = \beta_1(e/a) + \beta_2$.

The Tachiki-Maekawa theory provides a good explanation of how commensurate long period ordering may occur for a continuously varying electron concentration. Their calculation assumed that the configurational ordering resulted from a regular mixture of different domain sizes. Hence, they took M to be the average domain size. However, as I discuss in section III, their formula for the configurational energy corresponds to the exact result for Fujiwara phases for only integer values of M.

In this chapter the configurational energy is calculated assuming a Lorentzian pair potential function, but using the exact formula for the configurational energy. In addition, a more general minimization method will be used to determine the equilibrium configuration. This will provide the basis for investigating the two chief characteristics of the long period superstructures. These are the formation of long periods configuration that are Fujiwara phases and the stability of non-integer domain sizes.

The theoretical approach makes use of Khachaturyan's theory of maximum amplitude ordering [24]. The set of maximum amplitude configurations includes all Fujiwara phases and as well as non-Fujiwara type configurations. By performing the minimization over this set of configurations, it is shown that the Lorentzian potential leads to equilibrium long period superstructures that are Fujiwara phases.

According to Khachaturyan's theory, the wave vector of largest (dominate) superstructure reflection of the equilibrium phase will be located near the minimum of the pair potential function, but this wave vector will not

exactly correspond to the pair potential minimum because of energy contribution of the other less intense (non-dominate) superstructure reflections. This general principle is consistent with the results obtained by the calculation of Tachiki and Maekawa. Since the same general conclusions would be obtained using other pair potential functions with a similar shape, the use of the Lorentzian pair potential function is justified on the basis that the actual potentials for real long period superstructures are similar to a Lorentzian potential. Hence, using this potential I will demonstrate how the energy due to the non-dominated reflections leads to long period superstructures with stable non-integer domain sizes.

II. THEORY

A. Shift Function

Let us consider long period superstructures that are produced by a periodic sequence of displacements of a $L1_2$ unit cell as illustrated in figure 1b . The shift function $f(n)$ is defined to be equal to one if the nth cell is shifted by a displacement vector $a(0, \frac{1}{2}, \frac{1}{2})$, and zero otherwise. For example, the shift function for the structure shown in figure 1b takes on values

$$110011001001100110 \tag{2.1}$$

for $n = 0, 1, 2, \ldots 17$. The shift function specifies the configurational order of the long period superstructure.

B. Ordering Representation

The solute and solvent atoms are assumed to be distributed over the

sites of an FCC array. The long period superstructure under consideration have stoichiometry A_3B. Let the A atoms to be the solvent and the B atoms to be the solute.

The distribution function $p(n,i)$ defines the solute occupation probability at site i of the nth cell. The four sites within the FCC unit cell are shown in figure 2. Using the convention ,

$$i = \begin{cases} 1 & \text{for site } (0,0,0), \\ 2 & \text{for site } (\frac{1}{2},\frac{1}{2},0), \\ 3 & \text{for site } (0,\frac{1}{2},\frac{1}{2}), \\ 4 & \text{for site } (\frac{1}{2},0,\frac{1}{2}). \end{cases} \tag{2.2}$$

the solute distribution function can be expressed in terms of the shift function $f(n)$,

$$p(n,i) = \begin{cases} f(n) & \text{if } i = 4, \\ 1 - f(n) & \text{if } i = 3, \\ 0 & \text{if } i = 1 \textit{ or } 2. \end{cases} \tag{2.3}$$

The Fourier coefficients Q_k are defined by the formula

$$Q_k = \frac{1}{4L} \sum_{n=0}^{L-1} \sum_{i=1}^{4} p(n,i) e^{i2\pi k\cdot(n\hat{x}+b_i)} \tag{2.4}$$

where b_i is the basis vector for the ith site in the FCC unit cell and L is the period of the structure. Using equations $(2.2-4)$, one obtains

$$Q(k_x,k_y,k_z) = \frac{1}{4L} \sum_{n=0}^{L-1} [f(n) + (1-f(n))e^{i\pi(k_x+k_y)}]\, e^{i2\pi k_x} \tag{2.5}$$

where $k = (1/a)(k_x,k_y,k_z)$ and $r = a(x,y,z)$. Evaluating equation (2.3), the non-vanishing coefficients are

$$Q_{000} = Q_{100} = \frac{1}{4}, \tag{2.6a}$$

$$Q_{010} = Q_{001} = \frac{1}{4} - \frac{\sigma}{2L}, \tag{2.6b}$$

$$Q_{01\frac{s}{L}} = \frac{1}{2L}\sum_{n=0}^{L-1} f(n)e^{i\frac{2\pi}{L}sn}, \tag{2.6c}$$

where

$$\sigma = \sum_{n=0}^{L-1} f(n). \tag{2.6d}$$

C. Pair Potential Energy

Within the pair potential approximation, the configurational energy is

$$E = \frac{1}{2}\sum_{k\neq 0} V(k)|Q(k)|^2 \tag{2.7a}$$

where $V(k)$ is the Fourier transform of the real space pair potential function $V(r)$,

$$V(k) = \sum_{r} V(r)e^{2\pi k\cdot r}. \tag{2.7b}$$

The function $V(r)$ is the interaction energy $V_{AA} + V_{BB} - 2V_{AB}$ due to chemical mixing. Using equations (2.6-7), the energy is

$$E = \frac{1}{2}\left[V_{100}|Q_{100}|^2 + 2V_{010}|Q_{010}|^2 + \sum_{s=1}^{L-1} V_{01\frac{s}{L}}|Q_{01\frac{s}{L}}|^2\right] \tag{2.8}$$

Since the FCC fundamental cell experiences a tetragonal distortion, V_{100} and V_{010} are not necessarily equal. However, from equation (2.6a), Q_{100} is configuration independent. Hence, the value of V_{100} will not effect the minimization process.

D. Energy of Maximum Amplitude Configurations

For a given period L, there are 2^L possible configurations. As the period becomes larger, the number of configurations becomes much larger,

thus making it impossible to allow energy minimization calculations on a computer. Therefore, the minimization process is restricted to a subset of configurations that satisfy Khachaturyan's maximum amplitude criterion [24]. This criterion is such that, for a given concentration of A and B atoms, the configurational order is determined by maximizing the amplitude for one wave vector. This wave vector is called the dominant wave vector. In the case of the long period superstructures, the configurational order is defined by the one dimensional shift function $f(n)$. Hence, the ordering of unshifted and shifted cells is analogous to the ordering of A and B atoms on consecutive lattice planes. Thus, to construct the maximum amplitude long period superstructure, the amplitude of the dominant wave vector is maximized subject to the constraint that the fraction σ/L of unshifted cells is held constant.

For a given set of values for the integers s_0, L, and σ, the objective is to maximize the amplitude of the vector $(0, 1, \frac{s_0}{L})$. From equation (2.8), the configuration that maximizes $Q(0, 1, \frac{s_0}{L})$ is determined by maximizing the function

$$A_{s_0} = \left| \sum_{n=0}^{L-1} f(n) e^{i\frac{2\pi}{L} s_0 n} \right|^2 . \tag{2.9}$$

Since the shift function $f(n)$ takes on values one and zero, the quantity A will be maximized when $f(n)$ is chosen such that

$$A_{s_0} = \left| \sum_{I=0}^{\sigma-1} e^{i\frac{2\pi}{L} I} \right| . \tag{2.10}$$

This corresponds to

$$f(n) = \begin{cases} 1 & \text{if } (s_0 n) \; mod \; L < \sigma \; , \\ 0 & \text{if } (s_0 n) \; mod \; L \geq \sigma . \end{cases} \tag{2.11}$$

where the function $x \ mod \ y$ is the remainder of y divided into x. This implies that the amplitudes of the harmonics of the dominant wave are

$$Q_{01\frac{ms_0}{L}} = \frac{1}{2L}\left|\sum_{I=0}^{\sigma-1} e^{i\frac{2\pi}{L}mI}\right| \tag{2.12}$$

Using the formula,

$$\sum_{n=0}^{N} x^n = \frac{1-x^{N+1}}{1-x}, \tag{2.13}$$

equation (2.12) is summed to obtain

$$Q_{01\frac{ms_0}{L}} = \frac{sin(\pi\frac{m\sigma}{L})}{2L\ sin(\pi\frac{m}{L})}. \tag{2.14}$$

Equation (2.14) gives the amplitude spectrum of the maximum amplitude configuration with σ unshifted cells, a period L, and a dominant wave at $(0, 1, \frac{s_0}{L})$.

The wave vector $(0, 1, \frac{ms_0}{L})$ can be reduced to the first Brillouin zone using the identity $k \equiv k + H$ where H is a reciprocal lattice vector. Let s_m be defined by the relation

$$-1 < \frac{s_m}{L} < +1 \tag{2.15a}$$

where

$$s_m = ms_0 + 2n \tag{2.15b}$$

and n is the integer that puts s_m/L between the bounds ± 1. Then the equivalent wave vector for the mth harmonic of s_0 is

$$k_m = (0, 1, \frac{s_m}{L}) \equiv (0, 1, \frac{ms_0}{L}). \tag{2.16}$$

Using equations (2.8), (2.14), and (2.16), the energy is

$$E = \frac{1}{2}\left[V_{100}(\frac{1}{4})^2 + V_{010}(\frac{1}{4} - \frac{\sigma}{2L})^2 + \sum_{m=0}^{L-1} \frac{1}{4L^2} V_{01\frac{m}{L}} \frac{\sin^2(\pi \frac{m\sigma}{L})}{\sin^2(\pi \frac{m}{L})}\right]. \quad (2.17)$$

E. Energy Minimization

Let us suppose that the pair potential $V(0,1,k_z)$ has a well defined minimum at k_z^{min}. If the configurational energy was due solely to the dominant wave, one would expect the minimum energy configuration to have a dominant wave vector k_z^{dom} located at the minimum of the pair potential function, i.e., $k_z^{dom} = k_z^{min}$. However, the other non-dominant waves which result from the harmonics of the dominant waves also contribute to the energy. This may cause the dominant wave vector for the minimum energy configuration to be displaced away from the pair potential minimum. To illustrate this point, the pair potential function is chosen to have the Lorentzian form given in equation (1.4). The Lorentzian potential has two adjustable parameters, k_z^{min} and Δ. The parameter k_z^{min} determines the position of the minimum whereas the parameter Δ determines the sharpness of the potential function as illustrated in figure 3. Since the value of α in equation (1.4) will not effect the minimization of the energy provided it is positive, the parameter α is set to unity.

In the examples that to be presented, two energies will be plotted. The quantity E_{dom} is the energy neglecting the non-dominant ordering waves. This energy is obtained from equation (2.17) by truncating the term containing the sum over m at $m = 1$. The energy E_{tot} is the total energy obtained

by including all of the terms in equation (2.17). The points for E_{dom} and E_{tot} are plotted using circles and squares as markers, respectively.

1. Minimization with respect to σ

Let us first consider a superstructure with dominant wave vector $(0, 1, \frac{s_0}{L})$, and minimize the energy with respect to the number σ of unshifted cells. In figure 4, this is illustrated for $s_0/L = 5/18$ *and* $3/11$ with the Lorentzian parameters chosen to be $k_z^{min} = 5/18$ and $\Delta = .1$. Note that the minimum is at $\sigma/L = 1/2$ for even L and at the next nearest position to $\sigma/L = 1/2$ for odd L. Computer calculation shows that this result is obtained for most choices of s_0/L, Δ, and k_z^{min}. From the plotted energies in figure 4, one may note that the contribution of the non-dominant waves significantly increases the energy. However, the minimization of E_{dom} and E_{tot} lead to same value of σ.

2. Minimization set

To show how the dominant wave vector is related to the minimum position of the pair potential, a finite set of superstructures will be considered. This set is defined to be the set of maximum amplitude superstructures with period less or equal to 20. To eliminate redundancy, $k_z = s_0/L$ is required to be an irreducible fraction. For a given k_z^{min} and Δ, the energy is minimized with respect to σ. The energies $E_{dom}(s_0/L)$ and $E_{tot}(s_0/L)$ are plotted in figure 5 for $k_z^{min} = 5/18$ and $\Delta = .10$, and $.01$. An important point to note is the substantial effect of the non-dominant waves. The minimum of $E_{dom}(s_0/L)$ corresponds to the minimum of the pair potential function,

whereas a very different result is obtain for the minimum of $E_{tot}(s_0/L)$. In this case, the minimum may be displaced away from $k_z = k_z^{min}$. Moreover, as the value of Δ increases, the minimum of $E_{tot}(s_0/L)$ moves further away from minimum of the pair potential. Let us refer to the dominant wave vector $(01\frac{s_0}{L})$ of the equilibrium long period superstructure as $(01k_z^{equil})$. From figure 5b, one may note that this vector will be near to, but not necessarily equal to, the wave vector $(01k_z^{min})$.

3. Minimization with respect to k_z^{min}

The energy is minimized for different values of k_z^{min} for a fixed value of Δ. Again, the minimization is over the wave vectors listed in table 1. The z component of $k^{equil} = (01k_z^{equil})$ is plotted as a function k_z^{min}. The results of this minimization is shown in figure 6 for $\Delta = .01,\ .05,\ .50$. Note that as δ increases, fewer configurations are selected by the minimization process. An important characteristic of the result obtained is that variation k_z^{equil} with k_z^{min} is a step like function. That is, as k_z^{min} increases, k_z^{equil} increases in steps. As δ becomes smaller, the minimum of the pair potential becomes sharper. This leads to the steps becomes smaller. This result is evident by comparing the plots for the different values of Δ.

4. Minimization with respect to Δ

To further emphasize the effect of Δ, the minimization process is performed holding k_z^{min} constant and varying Δ. In figure 7, k_z^{equil} is plotted as a function of δ with $k_z^{min} = 5/18$. Note that for a sufficiently small Δ, k_z^{equil} converges to k_z^{min}. On the other hand, as Δ increases, the k_z^{equil} decreases

in steps towards $k_z = 1/4$.

III. DISCUSSION AND CONCLUSIONS

A. Fujiwara Phases

One of the most characteristic features of the long period superstructures is that their configurational order may be described by the Fujiwara square wave function given in equation (1.3). The Fujiwara phases are a subset of the Khachaturyan maximum amplitude superstructures. This result is apparent by comparing equation (1.3) and (2.11). Equation (2.11) defines the configurational order for maximum amplitude configurational with dominant wave vector at $(01\frac{s_0}{L})$ and σ unshifted cells. It can be put in the equivalent form

$$f(n) = \begin{cases} 1 & \text{if } \sin(2\pi\frac{s_0}{L}n) < \sin(2\pi\frac{\sigma}{L}) \ , \\ 0 & \text{if } \sin(2\pi\frac{s_0}{L}n) \geq \sin(2\pi\frac{\sigma}{L}) \ . \end{cases} \tag{3.1}$$

Note that for even L, equation (3.1) reduces to a square wave function for $\sigma/L = 1/2$. For odd L, the same result is obtained with σ being the integer for which σ/L is closest to $1/2$ since $f(n)$ is evaluated only for integer n.

The plots shown in figure 4 show that for a Lorentzian pair potential the minimum configurational energy is achieved with σ/L equal to $1/2$ for even L and σ/L nearest to $1/2$ for odd L. Note that from figure 4 that this result holds even when the minimum $(0, 1, k_z^{min})$ of the pair potential is not at the same position as the dominant wave vector $(0, 1, \frac{s_0}{L})$. The reason for this can be understood in general way by inspection of the amplitude formula for maximum amplitude superstructures given in equation (2.14).

The amplitude of the mth harmonic is proportional to

$$sin(\pi m \frac{\sigma}{L}). \tag{3.2}$$

For $\sigma/L = 1/2$, the amplitudes with odd m are non-vanishing. As σ/L is varied away from 1/2, the superstructure intensities decrease since they are proportional to the square of equation (3.2). Note that both the dominant and non-dominant intensities become smaller. Hence, since the pair potential $V(0, 1, k_z)$ is negative for all k_z, the configurational energy increases as σ/L is varied away from 1/2. Therefore, the configurational energy is minimized by a Fujiwara phase, i.e., $\sigma/L \rightarrow 1/2$.

In Fujiwara's original work on long period ordering, the existence of non-integer domain sizes was interpreted as a regular distribution of domain of different size. The square wave function given in equation (1.3) was used to generate a regular distribution of domains. The x-ray scattering amplitudes where calculated for different values of the half period of the square wave function. These amplitudes where then compared with the experimental data. From the distance between x-ray peaks, the half period M defined by equation (1.3) was measured. This quantity is widely used as a measure of the domain size.

While many theoretical studies have focus on the relationship between domain size and valence electron concentration, much less attention has been devoted to the issue of why the long period superstructures are Fujiwara's phases. That is, what is the theoretical rational of Fujiwara's assumption of regular mixing of domains?. Moreover, since there are different types of

regular mixing, why is the regular mixing specifically of the type defined by the Fujiwara square wave function?

In this chapter it has been shown that the regular mixing as defined in equation (1.3) occurs as a consequence of the minimization of the configurational energy. This is an important result because the widely accepted view point that the domain size corresponds to a change in periodicity due to a flatting of the fermi level does not explain the configurational ordering. This is because, as point out by Fujiwara, there are many different distribution that have similar ordering amplitudes with the the same value of M as determined by the separation distance between x-ray peaks.

B. Stability of Domain Size

The domain size M as defined by the Fujiwara square wave function in equation (1.3) corresponds to a maximum amplitude superstructure with dominant wave vector $(0, 1, \frac{1}{2M})$, i.e.,

$$M = \frac{L}{2s_0}. \tag{3.3}$$

This result follows from comparing equations (1.3) and (3.1). In figure 6, the z component k_z^{equil} of the dominant wave vector of the equilibrium superstructure is plotted as a function of the minimum position k_z^{min} of the pair potential. Since $k_z^{equil} = s_0/L$, the domain size is related to the dominant wave vector by the relation

$$2M = \frac{1}{k_z^{equil}}. \tag{3.4}$$

Hence, figure 6 shows that the domain size decreases in steps as k_z^{min} increases. The parameter Δ in equation (1.4) determines the sharpness of the

minimum of the Lorentzian potential. As Δ becomes larger, the minimum becomes less sharp, and the steps in domain size become bigger. Hence, the domain size M becomes more stable with respect to variations in k_z^{min} as potential minimum becomes broader.

The stability of the domain size can be conceptually understood in simple way using Khachaturyan's maximum amplitude principle [24]. This principle describes in a qualitative way the general relationship between the minimum in k-space of the pair potential function and the ordering wave vectors. Khachaturyan noted that in many ordered phases the wave amplitude is very large for one wave vector and much smaller for the other ordering wave vectors. Thus, he divides the ordering waves into two types - the dominant wave which has the largest amplitude, and the other waves which are called non-dominant waves. The configurational energy is the sum of two energies,

$$E = E_{DOM} + E_{ND}, \tag{3.5}$$

where E_{DOM} and E_{ND} are the energies associated with the dominant wave and non-dominant waves. The separation of the energy into these two terms assumes the energy result from pairwise interactions. If E_{ND} is neglected, the energy is minimized by placing the dominant wave vector at the position corresponding to the minimum of the pair potential function $V(k)$. As the period L increases, so does the number of dominant ordering waves, but these are less energetically favorable. Therefore, the system may decreases its energy by reducing the number non-dominant waves. This will cause the dominant wave vector to be near to, but not exactly at, the k-space

minimum of $V(k)$. Therefore, if the minimum of $V(k)$ is at $(s/L)H_0$ where H_0 is a reciprocal lattice vector, the configuration that minimizes the total energy may be at $(s'/L')H_0$ where $L' < L$ and $(s/L) \approx (s'/L')$.

The influence of the non-dominant waves is clearly evident in figure 5(b) where the energy versus dominant wave vector is plotted. Note that the energy E_{dom}, which is the energy neglecting the contribution of the non-dominant waves, has a minimum that coincides with the pair potential minimum at k_z^{min}. However, the total energy E_{tot} has a minimum that is shifted away from k_z^{min}. As the pair potential becomes broader, i.e, Δ increases, the difference between the equilibrium dominant wave vector k_z^{equil} and pair potential minimum k_z^{min} increases. This difference between k_z^{min} and k_z^{equil} results because of the energy contribution of the non-dominant ordering waves. In figure 5(a), the value of Δ is .01 which is ten times smaller than for value used in figure 5(b). In this case, k_z^{min} and k_z^{equil} are the same. This is because for $\Delta = .01$, the minimum of the pair potential function is very sharp as illustrated as figure 3.

C. Comparison with Experimental Data

In terms of the theory presented in this chapter, the dependence of the domain size on the electron concentration given in the empirical formula in equation (1.2) is explained by assuming that the minimum position of the pair potential is determined by the electron concentration. This is the assumption previously suggested by Tachiki and Maekawa. For example,

equation (1.3) corresponds to assuming

$$k_z^{min} = \frac{s_0}{L} = (e/a) - 1. \tag{3.6}$$

since $2M = L/s_0$.

If electron concentration were the sole factor determining domain size, one would expect the domain size to vary continuously with changes in composition. However, the long period superstructures in the Ag_3Mg and Al_3Ti alloys have been observed directly in the transmission electron microscope [18,19]. For these alloys long period superstructures with a very well defined crystallographic period are observed.

Tachiki and Maekawa had noted that for some systems such as Cu_3Pd, the domain size varies continuously with the electron concentration whereas for other alloys such as Pd_3Mg and Au_3Zn the domain size is fixed at $M = 2$ - that is, the domain size is constant over the composition range for which the alloy exist. Hence, their work sought to explain why an integer domain size may be stable with respect to changes in the electron concentration.

One may note from figure 6(c) that when $\Delta = .5$, the dominant wave vector $(01\frac{1}{4})$ which corresponds to $M = 2$ will minimize the configurational energy over a wide range of k_z^{min}. Hence, by equation (3.6) the $M = 2$ domain size will be stable over a wide range of electron concentration. For example, for the result plotted in figure 6(a) this range is

$$1.17 < (e/a) < 1.33. \tag{3.7}$$

Hence, for the alloy Cu_3Pd, the pair potential must have a broad minimum. On the other hand, if Δ is reduced by a factor of ten, thus making the

minimum of the pair potential much sharper, the range of stability is greatly reduced. If Δ becomes sufficiently small, then the domain will appear to vary continuously with the electron concentration.

These results reproduce the conclusions previously obtained by Tachiki and Maekawa for the case of integer domain sizes. The stability of non-integer domain sizes is now considered.

Superstructures with non-integer domain sizes are observed in Ag_3Mg and Al_3Ti. Moreover, for both of these systems a large number of different M values are observed. It has been shown that non-integer domain sizes that are fractions of the form $2M = L/s_0$ may be stable with respect to changes in k_z^{min} because of the influence of the non-dominant ordering waves. To predict exactly the long period superstructures in the Ag_3Mg and Al_3Ti would require a more precise knowledge of the pair potential function. Hence, the Lorentzian potential is regarded as a useful means of illustrating how the minimization of the energy leads to the stability of non-integer domain sizes. For the long period superstructures in the $Al-Ti$ and $Ag-Mg$ systems, this work suggest that the pair potential minimum is sharper than for Cu_3Pd but not as sharp as systems where incommensurate long period ordering occurs.

The superstructures in the $Al-Ti$ alloy are observed over a narrow composition range of $71-73\%$ Al [19]. The phase diagram for the $Al-Ti$ system shows that this range corresponds to the single phase region of the Al_3Ti type phase [25]. Hence, it is not possible to vary the composition

of the long period superstructures in $Al - Ti$ by more than a few percent. However, a large number of different domain sizes are observed by varying the temperature. Amelinckx et al. obtains the results given in figure 8. The different domain sizes at each temperature result from different compositions of the samples. Note that the largest effect is the variation of domain size with temperature. This cannot be explained by assuming that k_z^{min} is solely a function of the valence electron to atom ratio as in equation (3.6).

To explain how the temperature dependence of the domain size may be explained with the context of the theory presented in this chapter, let us digress briefly to discuss the origin of the pair potential function. The theoretical approach assumed that the solute and solvent atoms are distributed over the sites of a FCC array. Hence, the quantity $V(k)$ is obtained by performing the discrete Fourier transform of the real space pair potential $V(r)$,

$$V(k) = \sum_r V(r)\, e^{i2\pi k \cdot r}. \tag{3.8}$$

where the sum is over the sites of FCC array. Actually, in the case of the long period superstructures, the FCC array is an idealization since the subcell is a tetragonally distorted FCC array. Then, the points in space for which $V(r)$ is sampled is a function of the lattice parameters a and c of the subcell. Suppose that the real space interaction pair potential is a function of the electron density ϵ. Then, the Fourier quantity $V(k)$ is function of electron concentration and subcell lattice parameters, i.e.,

$$V(k) = V(k; \epsilon, a, c). \tag{3.9}$$

Hence, the k-space position of the $V(k)$ minimum is a function of the same

parameters,

$$k_z^{min} = k_z^{min}(\epsilon, a, c). \tag{3.10}$$

The expansion of the crystal with increasing temperatures changes the the subcell lattice parameters. By equation (3.10), this causes the $V(k)$ minimum to shift its position. Therefore, it would be reasonable to assume that the k_z^{min} is a function of both electron density and temperature.

The data shown in figure 8 implies that the k_z^{min} decreases as the temperature is raised. At higher temperatures, a larger number of domain sizes is observed. Hence, this indicates that the pair potential minimum becomes sharper as the temperature increases. As already shown, as the pair potential minimum becomes broader, i.e., Δ becomes bigger, the domain size is stable against larger variations in k_z^{min}. Hence, the long period superstructure with domain size M will be stable against larger variations of both composition and temperature. This prediction is consistent with the observations of Amelinckx et al.

D. Maximum Amplitude Principle

In part A of this section it was shown that the Fujiwara phases satisfy Khachaturyan criterion for maximum amplitude ordering. This result is significant because the maximum amplitude principle is very general. In this chapter it has been demonstrated how maximum amplitude ordering leads to stable non-integer domain sizes using the pair potential approximation. It is likely that the same conclusion could be achieved by performing the same calculations using a solid state physics approach. For example,

for each maximum amplitude configuration, the energy could be computed from a band structure calculation or pseudopotential theory. Computing the energy in this manner instead of equation (2.17) and employing the same minimization procedure, the stability of non-integer domain sizes could be investigated at a more fundamental level.

When superstructure ordering occurs with period L, the bands of the fundamental structure are split into L bands. This leads to a change of energy due to the introduction of additional band gaps. From this point of view, the formation of long period superstructures with a rational fraction non-integer domain size results from a lowering of the energy due to reducing the number of bands. This would stabilize the crystallographic period of superstructures with non-integer domain sizes. Moreover, the most energetically favorable coupling between the electrons and the array of atomic ion cores is likely to occur when the dominant ordering wave vector corresponds to the band gap that leads to the greatest reduction in electronic energy. Hence, it is quite possible that the use of maximum amplitude principle, which was originally derived by Khachaturyan using the theoretical framework of a pair potential model, may also be explained in the case of the long period superstructures by a calculation of the energy using solid state theory.

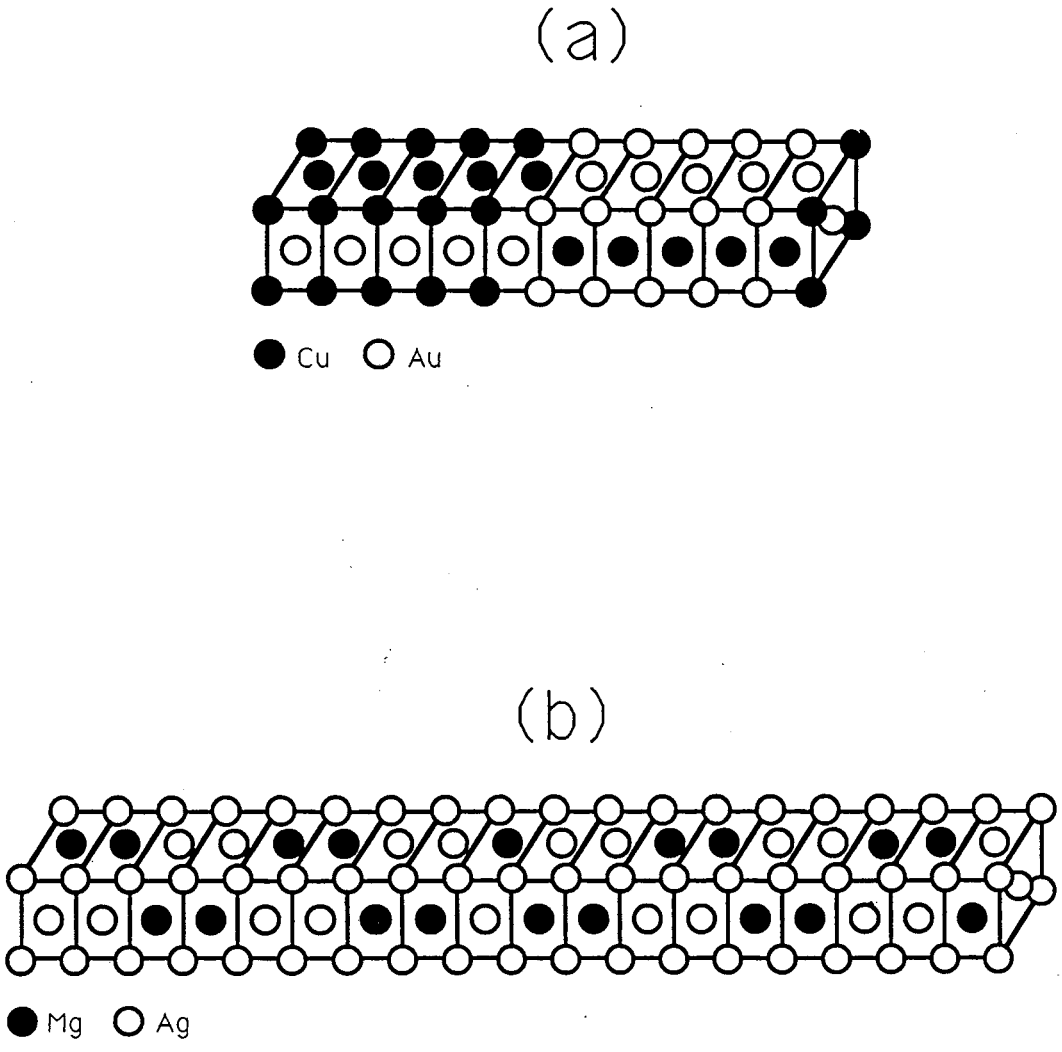

Figure 1. Long period superstructures $CuAu(II)$ (a) and Ag_3Mg (b).

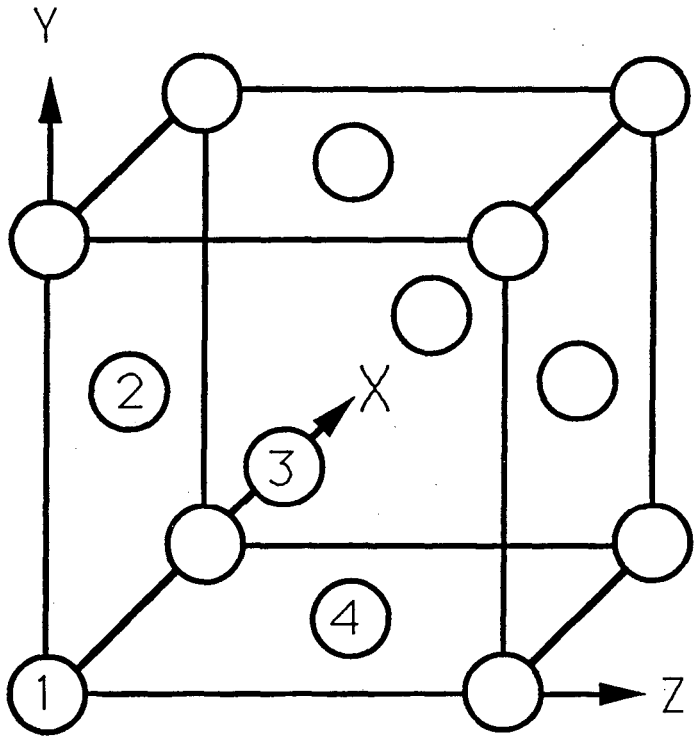

Figure 2. Basis positions of face centered cubic (FCC) unit cell.

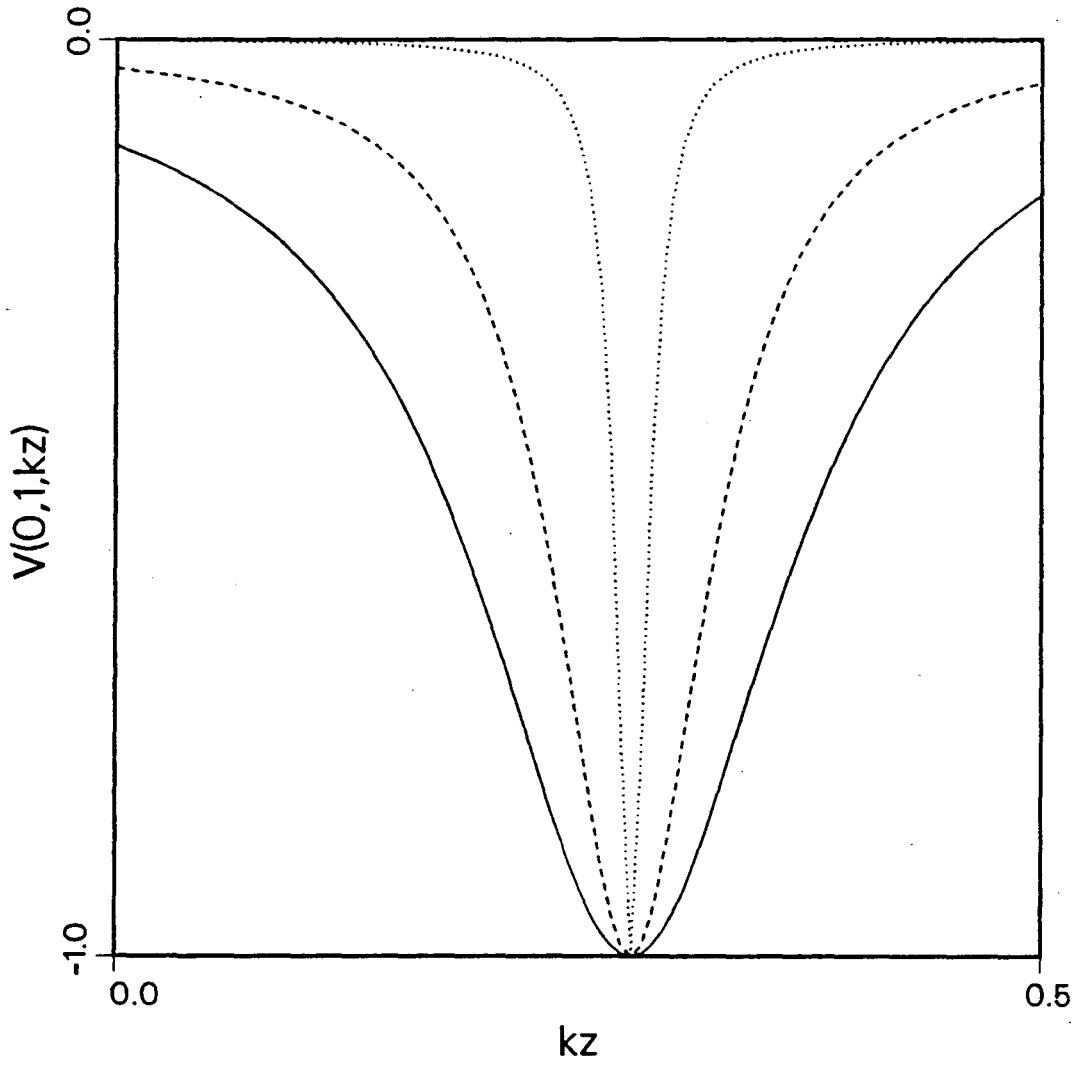

Figure 3. Lorentzian potential as function of k_z for $\Delta = 0.1$ (solid line), 0.05, (dashed line) and 0.01 (dotted line).

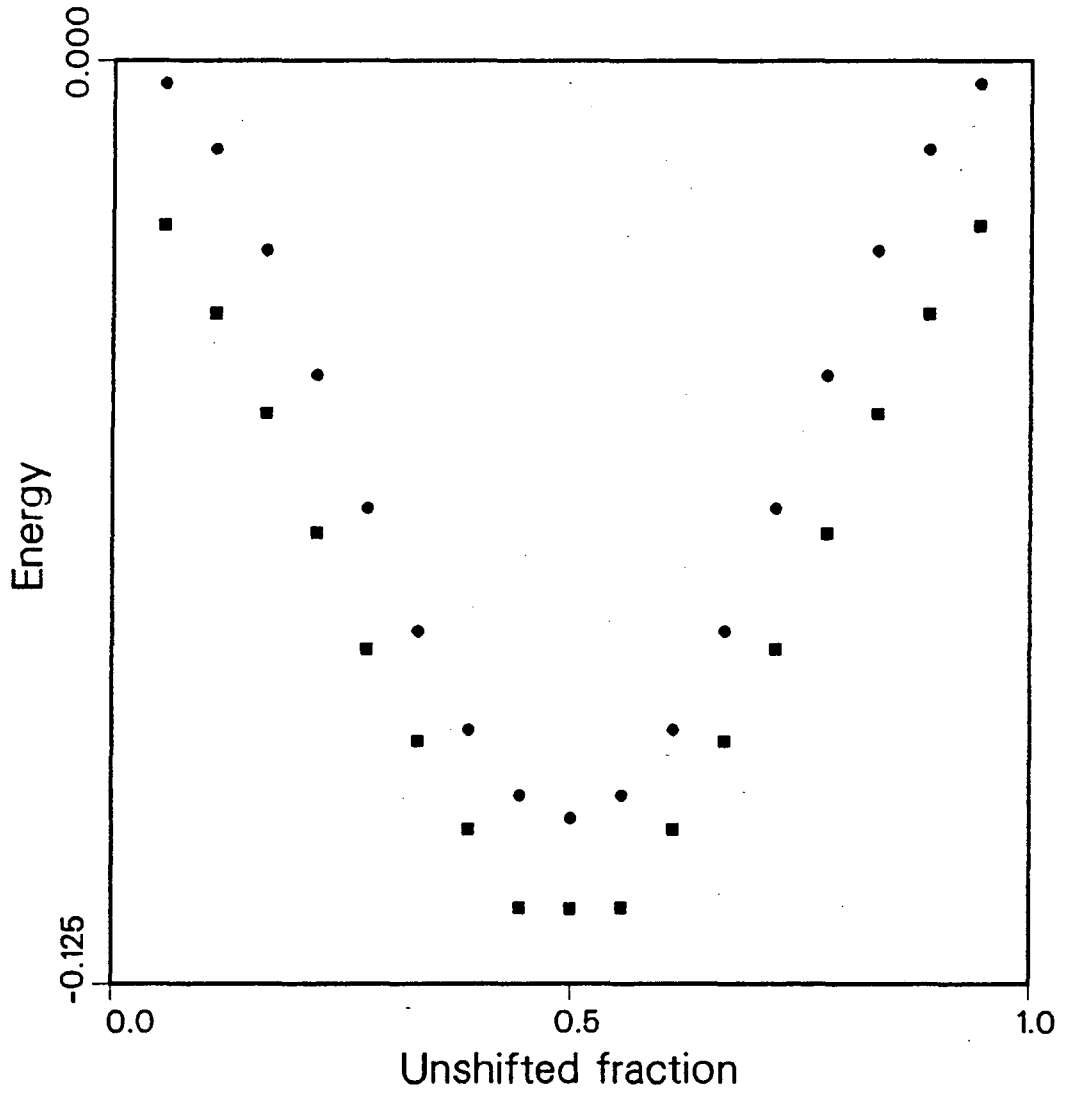

Figure 4(a). Dominant energy, E_{dom}, (circles) and total energy, E_{tot}, (squares) vs. fraction of unshifted cells, σ. Energy is computed with pair potential parameters $k_z^{min} = 5/18$, and $\Delta = 0.1$. The dominant wave vector is $(0, 1, \frac{5}{18})$.

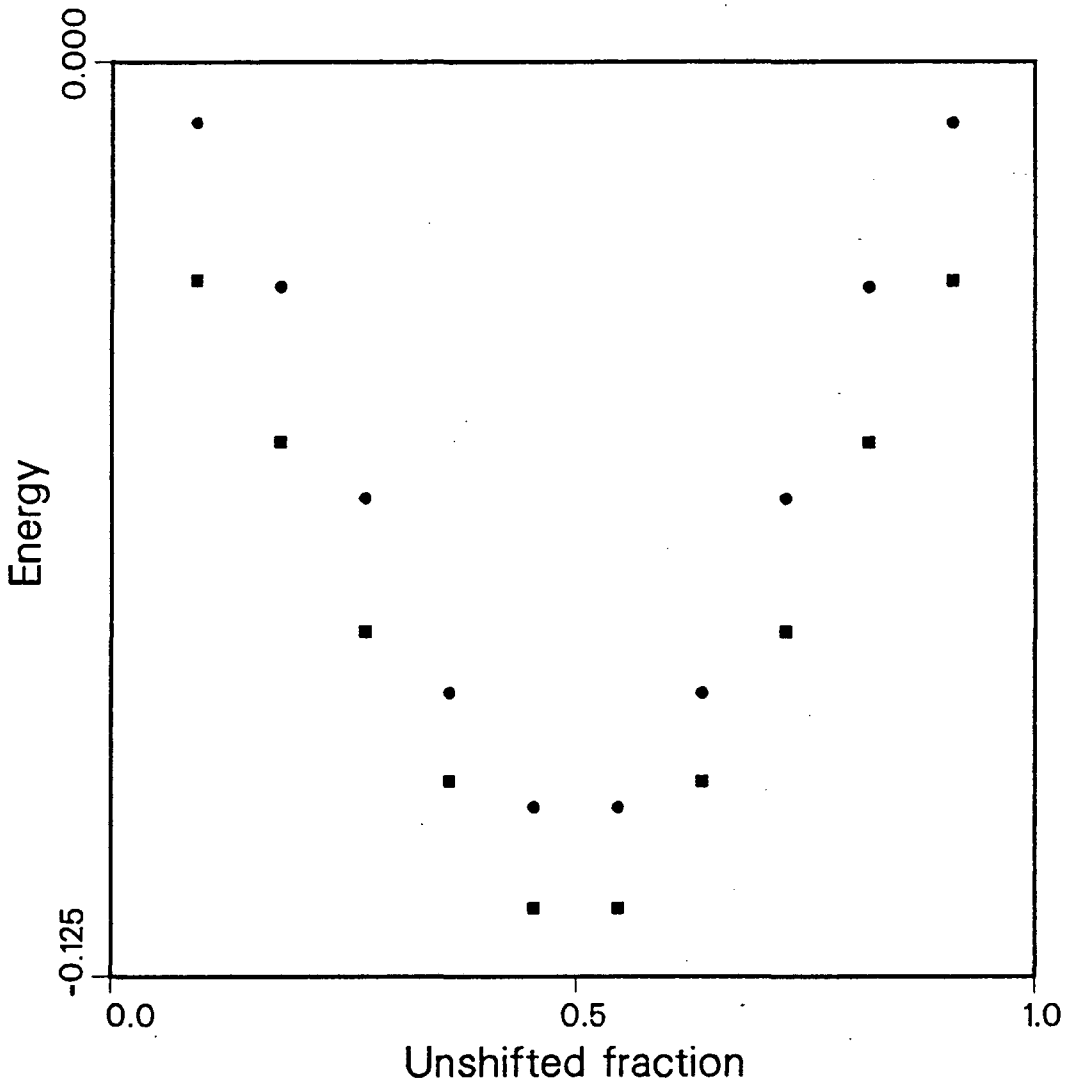

Figure 4(b). Dominant energy, E_{dom}, (circles) and total energy, E_{tot}, (squares) vs. fraction of unshifted cells, σ. Energy is computed with pair potential parameters $k_z^{min} = 5/18$ and $\Delta = 0.1$. The dominant wave vector is $(0, 1, \frac{3}{11})$.

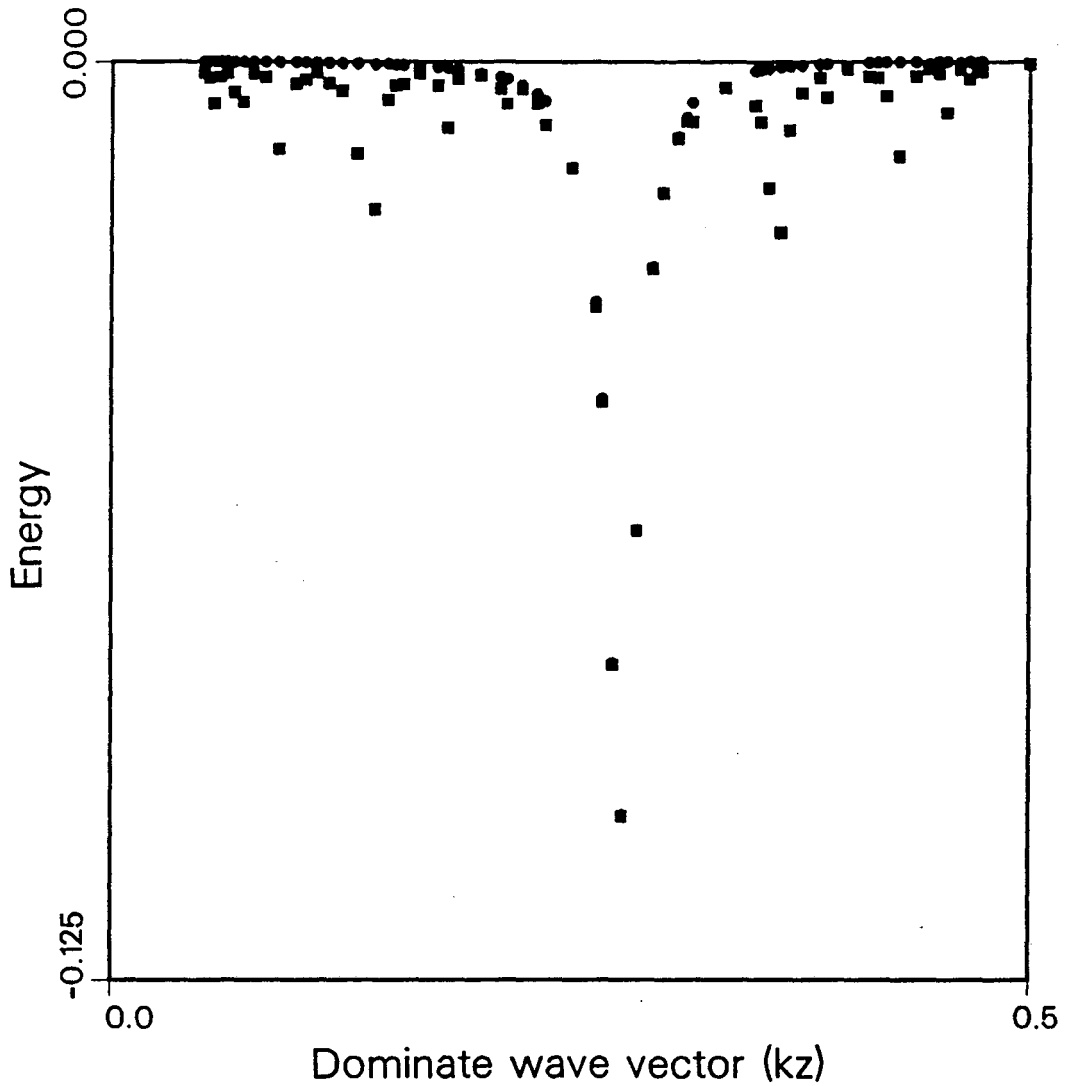

Figure 5(a). Dominant energy, E_{dom}, (circles) and total energy, E_{tot}, (squares) vs. dominant wave vector $(0, 1, k_z)$ for $k_z^{min} = 5/18$ and $\Delta = 0.01$.

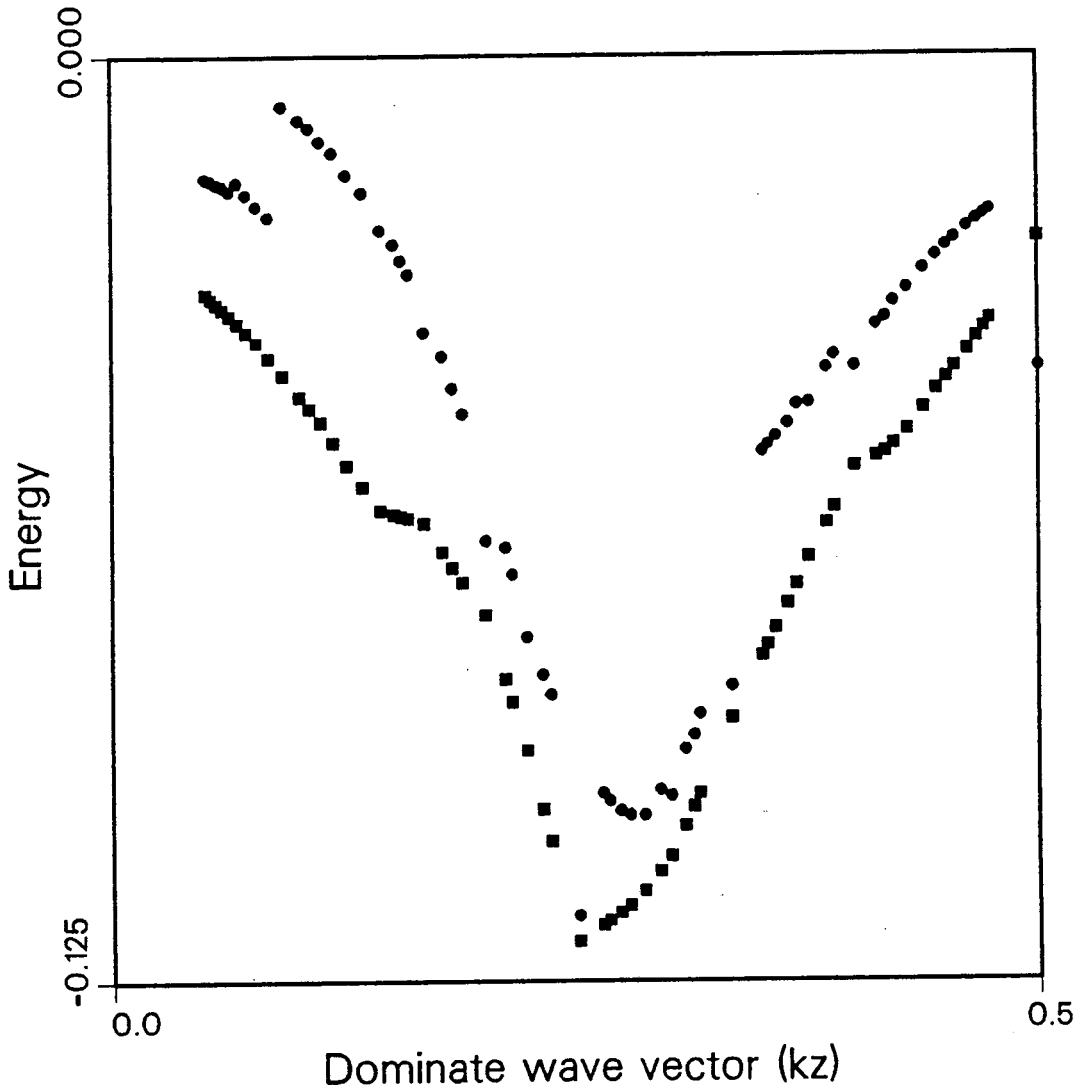

Figure 5(b). Dominant energy, E_{dom}, (circles) and total energy, E_{tot}, (squares) vs. dominant wave vector $(0, 1, k_z)$ for $k_z^{min} = 5/18$ and $\Delta = 0.1$.

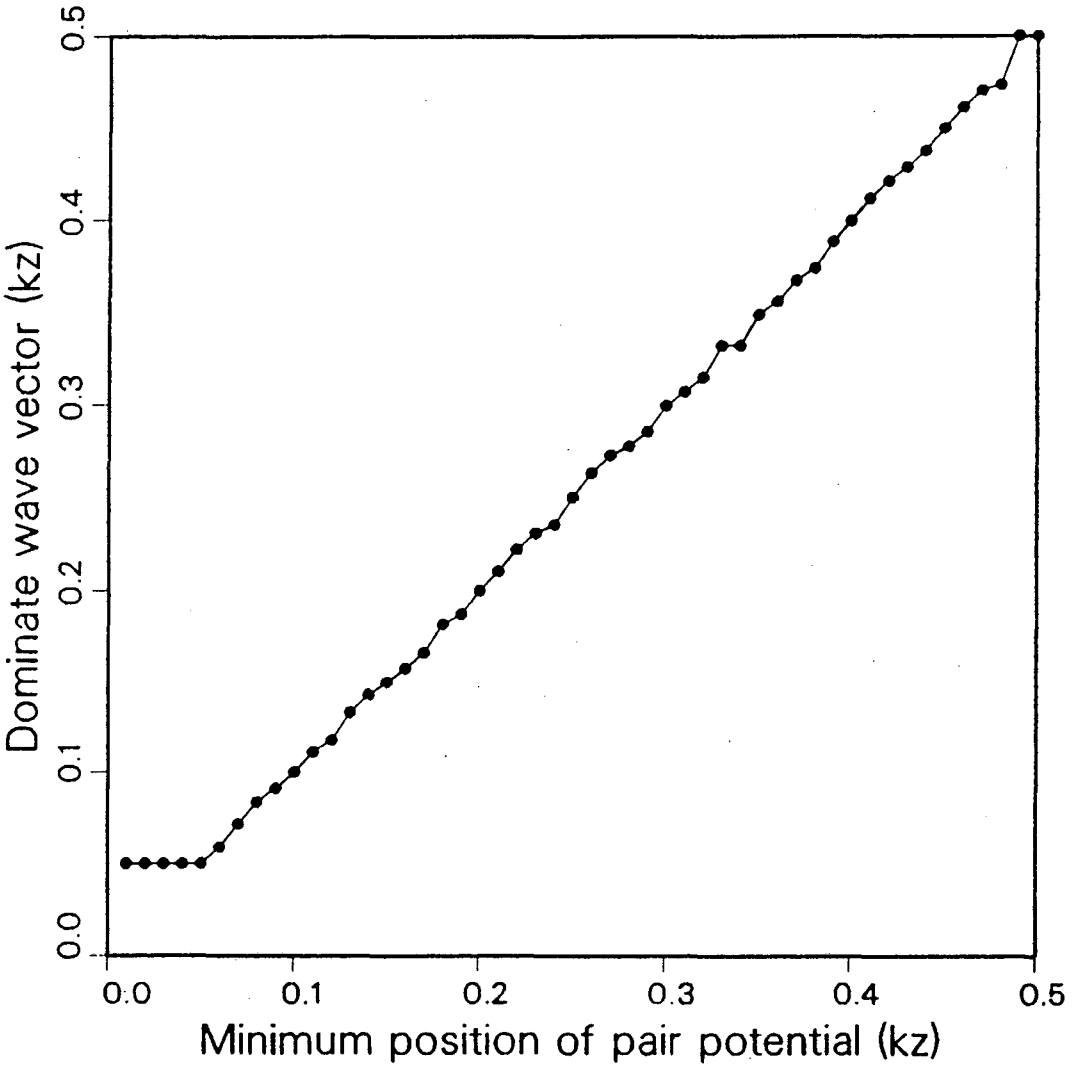

Figure 6(a). Dominant wave vector $(0, 1, k_z)$ vs. pair potential minimum position $(0, 1, k_z^{min})$ for $\Delta = 0.01$.

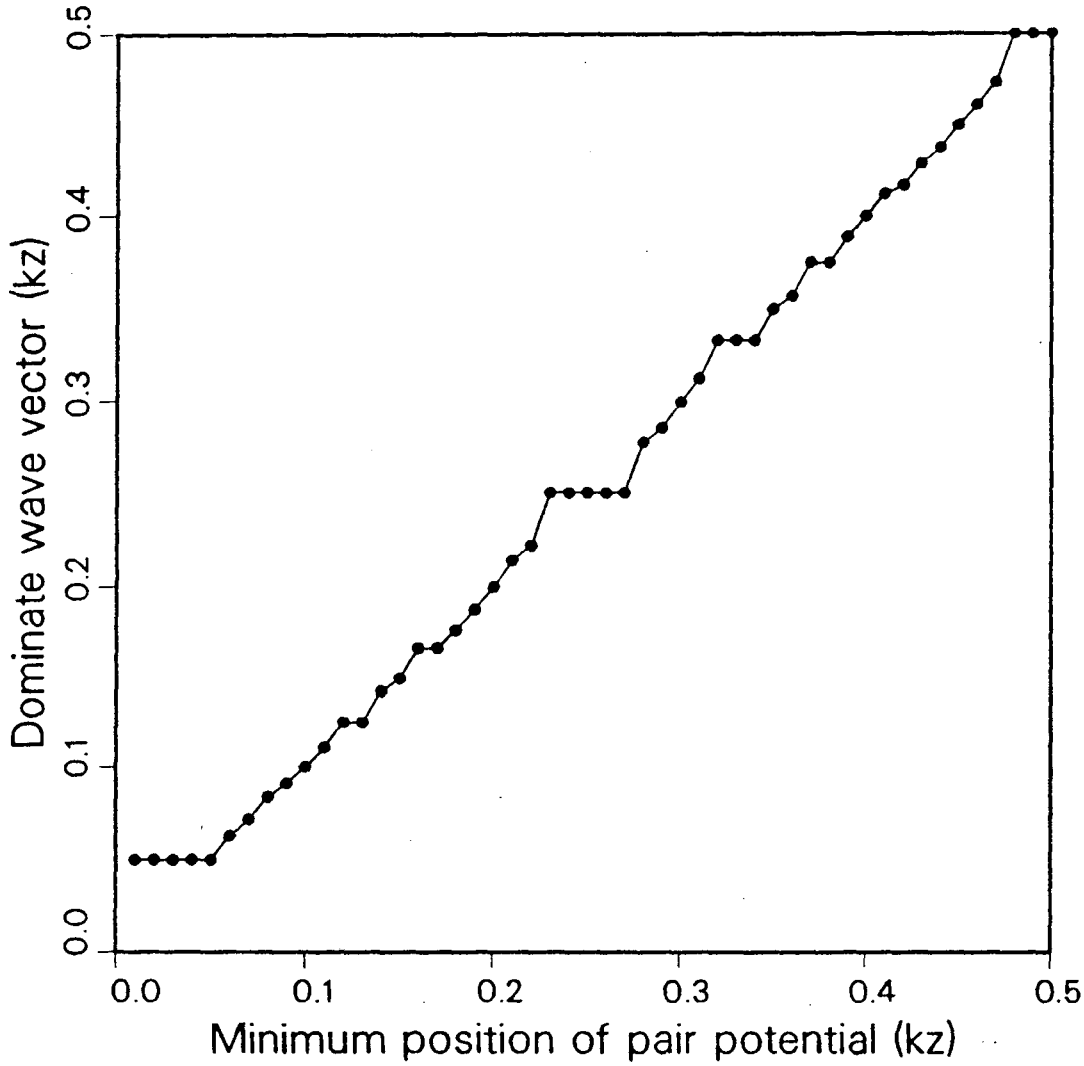

Figure 6(b). Dominant wave vector $(0, 1, k_z)$ vs. pair potential minimum position $(0, 1, k_z^{min})$ for $\Delta = 0.05$.

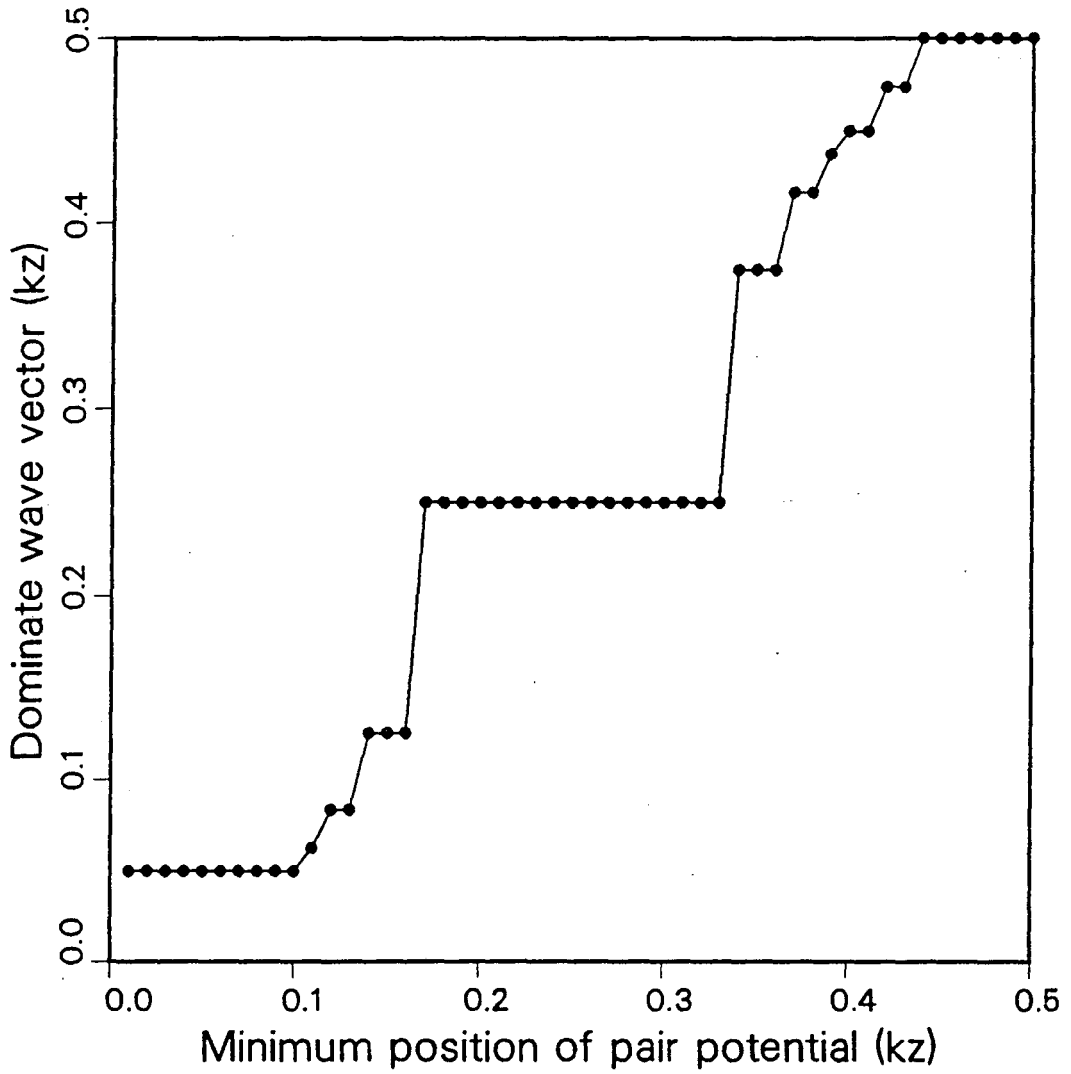

Figure 6(c). Dominant wave vector $(0, 1, k_z)$ vs. pair potential minimum position $(0, 1, k_z^{min})$ for $\Delta = 0.1$.

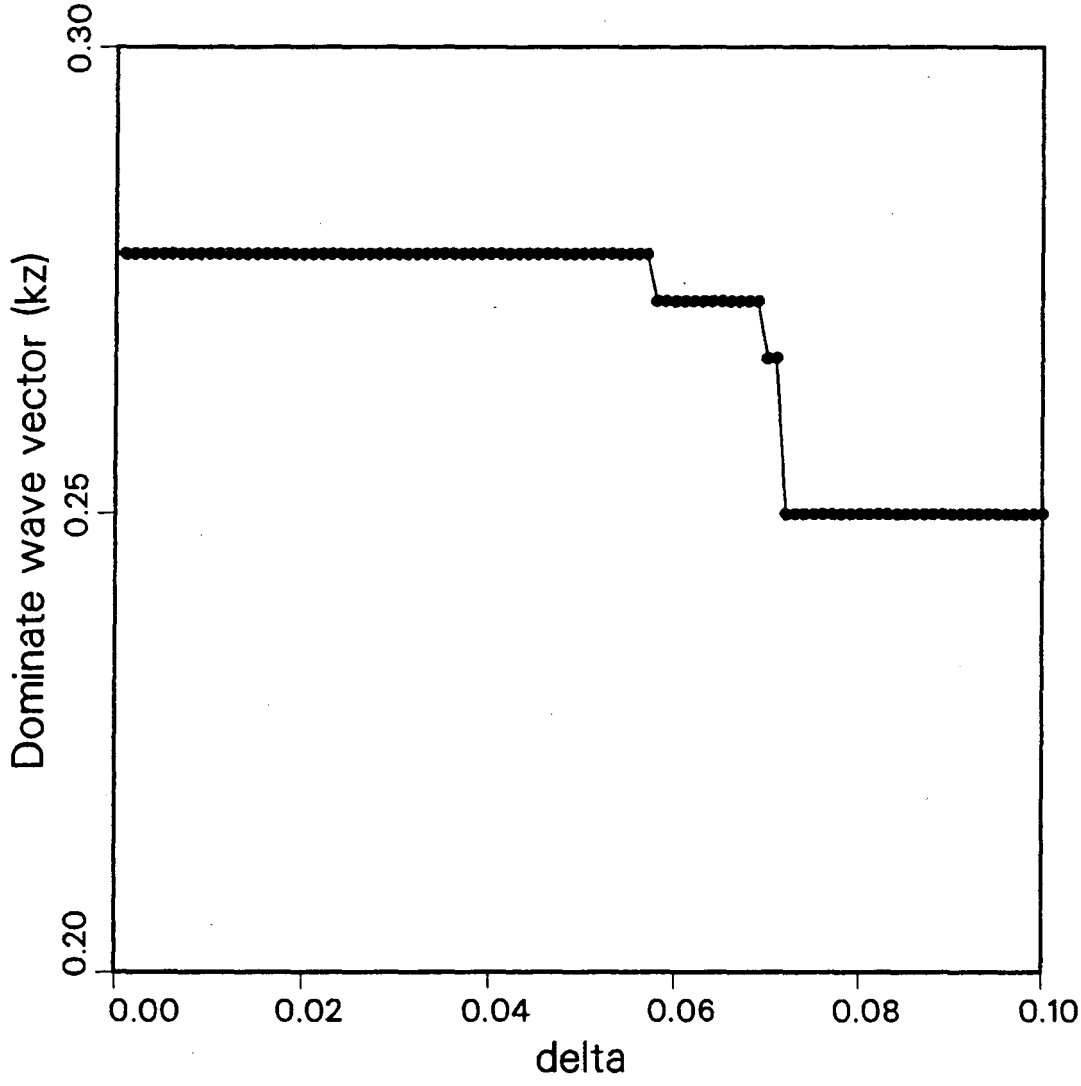

Figure 7. Dominant wave vector $(0, 1, k_z)$ vs. pair potential parameter Δ for $k_z^{min} = 5/18$.

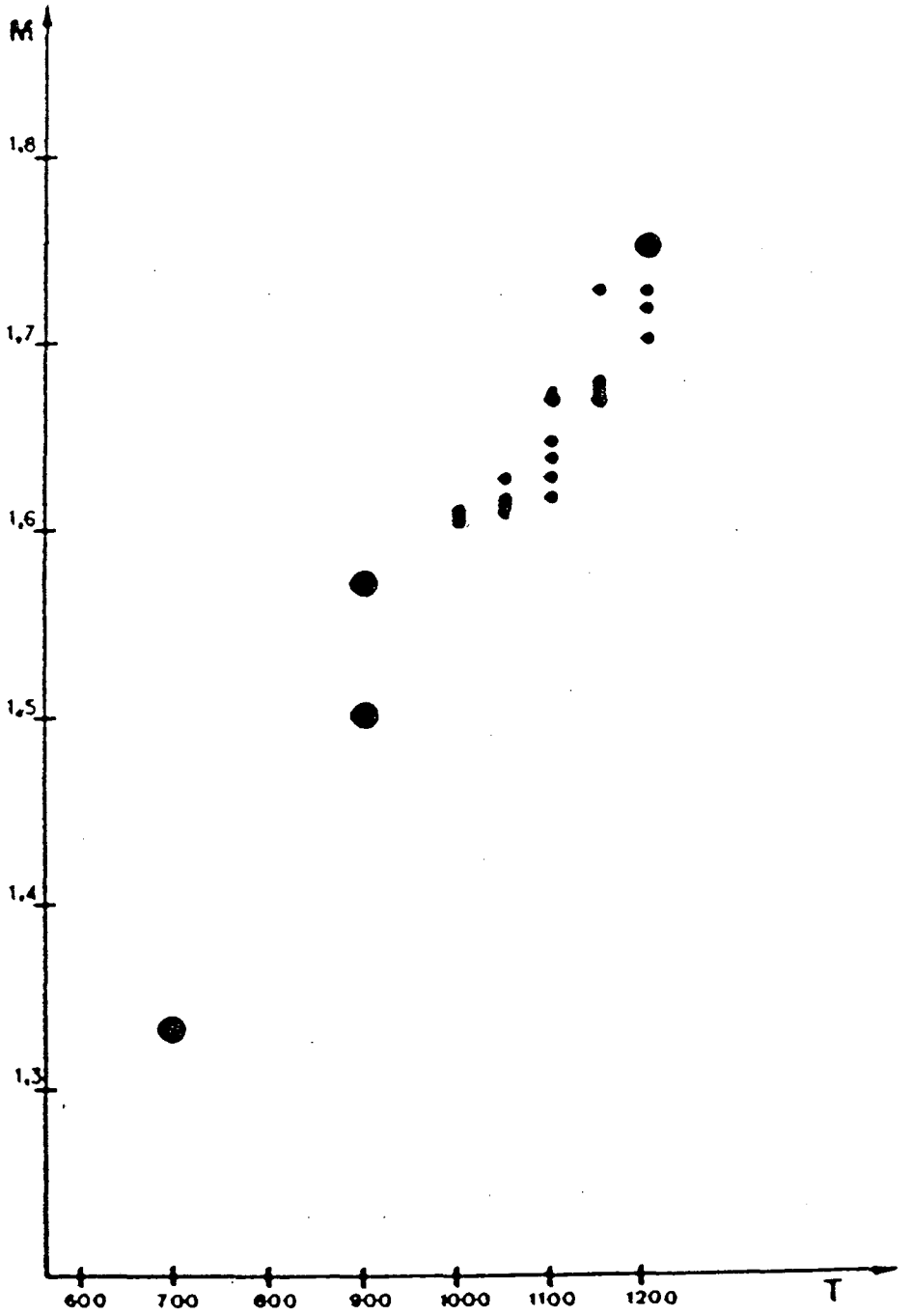

Figure 8. Domain size vs. temperature data obtained by Amelinckx et. al.

CHAPTER 3

CATION ORDERING IN CALCITE AND DOLOMITE

This chapter presents a theoretical investigation of the cation ordering in calcite and dolomite. It is shown that the ordering may be treated as a distribution of cations over the sites of a pseudocubic FCC array. This provides the basis for an analogy with FCC based metal alloys. The theoretical analysis shows that there is an isomorphic relationship between the precipitate phases in calcite and dolomite and the special point superstructures in the $Cu-Au$ and $Cu-Pt$ alloy systems. Assuming pairwise interactions, the conditions for homogenous ordering equilibrium and ordering wave instabilities are determined. Using the quantity $V(k)$, which is the Fourier transform of the interaction pair potential $V(r)$, it is shown that the observed precipitates in calcite and dolomite are consistent with the assumption that $V(k)$ has minima at the special point positions $\{1,0,0\}$ and $\{\frac{1}{2},\frac{1}{2},\frac{1}{2}\}$ respectively.

I. INTRODUCTION

The ordered superstructures that appear as precipitates in ferroan dolomite (ankerite) and calcite were recently studied by Wenk et.al. by electron microscopy [26]. Their samples were obtained from an aggregates of calcite and dolomite that formed in the cavity of an ammonite snail shell. The calcite and dolomite regions are believed to have formed from an aqueous solution millions of years ago. One possible mechanism of precipitate formation is that of an ordering transformation from a phase where the

cations are randomly distributed over the Ca sites of the calcite structure. However, since the disorder to order temperature is well above the temperature where aqueous growth may occur, this mechanism is not very likely. To explain how the precipitate phases may have formed, it is suggested in this chapter that the initial growth at the mineral to aqueous solution interface is followed by an ordering wave instability which produces a spontaneous formation of precipitates. Since this transformation can occur near the surface where the kinetics are favorable, the precipitates become frozen within the bulk.

The theoretical approach is based on the isomorphic relationship between the cation ordering in the rhombohedral carbonates and the substitutional ordering in face centered cubic (FCC) based metal alloys. In particular, the ordered rhombohedral carbonate phases are described as a distribution of cations over the sites of a pseudocubic FCC array. Subsequently, by analogy with FCC based ordering in metals, the ordering wave method is used to investigate the conditions for homogenous phase equilibrium and ordering wave instabilities.

The configurational energy in FCC based alloys is often modeled by assuming that the solute and solvent atoms interact by means of an interaction pair potential $V(r)$. An important quantity in the ordering theory of FCC based superstructures is the quantity $V(k)$, which is the Fourier transform of the pair potential function $V(r)$. The points of isolated symmetry in the reciprocal space of the FCC fundamental lattice are known as the Lifshitz special points, named after Lifshitz, who first discussed their significance

for transitions of the second kind [12]. Clapp and Moss [14] showed that pair potential $V(k)$ function can be deduced from x-ray diffuse scattering data. Additionally, they concluded for the alloys $Au - Cu$ and $Zn - Cu$, the minima of $V(k)$ are at special point positions in reciprocal space. They also showed that thermodynamic requirement of energy minimization will often produce a special point superstructure, if the minima of $V(k)$ are at special point positions in reciprocal space. The special point superstructures are defined to be ordered structures that have ordering wave vectors that are located at the special point in reciprocal space. This conclusion that the special point superstructures in FCC based metal alloys occur as a consequence of special point $V(k)$ minima has become widely accepted [11].

Since the cation array is a pseudocubic FCC array, the cation distributions in the rhombohedral carbonates may be described as FCC based ordered phases [26]. With the exception of one phase, all of the ordered rhombohedral phases in calcite and dolomite are special point superstructures. However, the dominant ordering wave vector (largest amplitude wave) for the exception is a special point wave vector. Since all of these phases contain special point ordering waves, the occurrence of these phases is explained by assuming that the cation interaction pair potential has minima at special point positions in reciprocal space. Hence, the aim of this chapter is to explain the special point ordering for the cation distributions in the rhombohedral carbonates using the same theoretical approach that is used for FCC based metal alloys.

By a consideration of the equilibrium conditions for homogenous order-

ing, it is shown that the ordered precipitates in calcite are consistent with pair potential minima at the special point positions $\{1,0,0\}$, whereas the ordered precipitates in dolomite are consistent with pair potential minima at the special point positions $\{\frac{1}{2},\frac{1}{2},\frac{1}{2}\}$. Khachaturyan has shown that the highest temperature ordering wave instability will have wave vectors corresponding to the minima of the pair potential function $V(k)$ [11]. Moreover, these ordering waves will be the most energetically favorable, and thus will have the most rapid rates of formations out of the disordered state. Hence, the existence of the special point $V(k)$ minima in calcite and dolomite offers a simple explanation of the observed ordered rhombohedral carbonates phases in these minerals.

The interaction pair potential for a mixing of A and B atoms is

$$V(r) = V_{AA}(r) + V_{BB}(r) - 2V_{AB}(r) \tag{1.1}$$

where $V_{IJ}(r)$ is the potential between atoms of type I and J separated by a distance r . Since ordering species are Ca and Mg for calcite, the interaction pair potential is

$$V(r) = V_{CaCa}(r) + V_{MgMg}(r) - 2V_{CaMg}(r). \tag{1.2}$$

The ordering species in ferrroan dolomite (ankerite) are Ca, Mg and Fe, thus the cation ordering is ternary. However, since the Mg and Fe disorder over the same sites, the ordering in dolomite may be treated as a pseudobinary ordering of Ca and X where X is (Mg, Fe). In this case

$$V(r) = V_{CaCa}(r) + V_{XX}(r) - 2V_{CaX}(r). \tag{1.3}$$

Hence, the result that the $V(k)$ minima are at different special point ordering stars for calcite and ferroan dolomite is due to the difference in their pair potentials as defined by equations (1.2-3).

The central aspect of the theoretical development in this chapter is the analogy between the cation ordering in the rhombohedral carbonates and substitutional ordering in FCC based alloys. Therefore, the theory section begins by describing why the cation ordering may be treated as a distribution over a pseudocubic FCC array. Further discussion will explain the relationship of ordered phases in calcite and dolomite to ordered phases in metal alloys. The ordering wave description of the ordered rhombohedral carbonated phases is developed using the pseudocubic cation FCC ordering frame. The ordering wave representation provides a means of determining the conditions for homogenous equilibrium. Using the result obtained from the equilibrium analysis, I describe how the ordered cation distributions may result from an ordering wave instability.

In the discussion section, I describe how the results of the theory section offer a new perspective on how the precipitate phases in calcite and dolomite may have formed. In particular, I will argue that the special point ordering wave instabilities provide a thermodynamically and kinetically favorable mechanism of producing the cation ordering in the observed rhombohedral carbonate phases.

II. THEORY

A. Isomorphism with FCC Based Ordering

The ordered phases that will be considered are superstructures of the calcite structure. The crystal structure results from the packing of carbonate groups and smaller metal ions. As shown in figure 1, the carbonate ions lie in the basal plane of the hexagonal calcite unit cell and have two orientations which alternate back and forth. The metal ions are surrounded by octahedral arrangement of oxygen atoms. The cation ordering results from the distribution of metal ions over the sites of these octahedrally coordinated positions. Hence, the carbonate groups play a passive role in that their oxygen atoms serve only to provide interstitial sites for the cations.

The calcite structure is a distorted $NaCl$ structure where the Na sites are occupied by metal cations and the Cl sites by carbonate anions. The CO_3 molecules are almost planar and lie in the $< 1,1,1 >$ plane of the cubic unit cell for $NaCl$. This introduces a distortion in the $< 1,1,1 >$ direction. If this distortion is neglected, the cation sites define a pseudocubic FCC array. Therefore, since the carbonate ions have a passive effect on the cation ordering, the cation ordering is analogous to the ordering of metal atoms in FCC based alloys. This is an important result that I wish to emphasize. Since both the cation ordering in the rhombohedral carbonates and the substitutional ordering in FCC based metal alloys may be described as a distribution over the sites of a pseudocubic FCC array, these two types of ordering are isomorphic.

The site positions and occupancies of the cations for the rhombohedral carbonate phases are given in table 1. The cation distributions are illustrated in figure 2 using a hexagonal cell, and in figure 3 using a pseudocubic cell. The transformation from the hexagonal coordinate system to a pseudocubic coordinate system is achieved using the relations

$$A = (1,0,0)_{hex} = (-1,0,1)_{cub} \tag{2.1}$$

$$B = (0,1,0)_{hex} = (-1,1,0)_{cub} \tag{2.2}$$

$$C = (0,0,1)_{hex} = (2,2,2)_{cub} \tag{2.3}$$

These relations are obtained in the following way. The basal plane of the hexagonal unit cell corresponds to the $< 1,1,1 >$ plane of the FCC pseudocubic frame. Since the basis vectors A and B define the basal plane of the hexagonal cell, they must lie in the $< 1,1,1 >$ plane of the FCC pseudocubic frame. The close packed directions in a FCC frame are $\frac{1}{2}\{1,1,0\}$. Hence, by inspection of figure 3, the basis vectors for the basal plane of the hexagonal cell may be chosen to be $(-1,0,1)$ and $(-1,0,1)$, since these vectors are in the $< 1,1,1 >$ plane and correspond to displacements equal to twice the distance in the close packed direction. In the hexagonal cell, there are six layers of cations, each layer being parallel to the basal plane. In a FCC crystal the normal direction from one $< 1,1,1 >$ plane to the next is $(1/3)(1,1,1)$. Hence, the C axis basis vector for the hexagonal cell corresponds to $(2,2,2)$ in the FCC pseudocubic frame.

The hexagonal and pseudocubic coordinate systems provide an equivalent means of describing the cation ordering, but the isomorphism with FCC

based metal alloys is easier to see using the pseudocubic coordinate system. As shown in figure 3, the calcite phase (α) is the fundamental structure and is analogous to a FCC structure. The dolomite structure (β) and precipitate phase γ are isomorphic with the $CuPt$ and $CuPt_3$ phases, respectively. On the other hand, the ν and μ precipitate phases are isomorphic phases with the $CuAu(I)$ and Cu_3Au phases, respectively. For the δ precipitate phase, there is no isomorphic metal alloy phase, but this phase can still described as an isomorphic superstructure of the FCC superstructure.

The fact that the matrix phases β and α, and the precipitate phases γ, μ, and ν are isomorphic with known metal alloy phases suggests that the theoretical explanation of the cation ordering can be developed by analogy with ordering in metals. To emphasize this point of view, I will find it useful to refer to the cation distributions for the different rhombohedral carbonate phases by association with their corresponding isomorphic metal alloy phases, i.e., the matrix phases are α (FCC) and β ($CuPt$). Similarly, the precipitate phases are γ ($CuPt_3$), ν ($AuCu$), μ (Cu_3Au), and δ (A_2B). For the δ phase, I will use the generic notation A_2B since this phase has no corresponding isomorphic FCC based metal alloy phase.

B. Ordering Wave Description

For a binary alloy, the ordering species are of two types. One is taken to be the solute, and the other the solvent. Let the probability of a site r of the FCC array being occupied by a solute atom be denoted as $p(r)$. The values of solute probability taken over all the sites of the FCC array

defines the probability function $p(r)$. The Fourier transform of the solute probability function is

$$p(r) = \sum_k Q(k)\, e^{i2\pi k\cdot r} \tag{2.4}$$

where the Fourier coefficients $Q(k)$ are defined by the relation

$$Q(k) = \frac{1}{N}\sum_r n(r)\, e^{-i2\pi k\cdot r}. \tag{2.5}$$

This sum is computed over the N sites of the unit cell. The Fourier amplitude $Q(k)$ is regarded as the amplitude of the ordering wave

$$p_k(r) = Q(k)\, e^{-2\pi k\cdot r}. \tag{2.6}$$

From this point of view, the ordered superstructures results from a superposition of ordering waves.

Since the conventional unit cell of the FCC array is cubic with edge length a, one may define the real space positions to be

$$r = a(x, y, z) \qquad (2.7).$$

The wave vectors are then defined by the relation

$$k = \frac{2\pi}{a}(k_x, k_y, k_z) \tag{2.8}$$

where a is the length of the FCC unit cell. Let us regard the Ca atoms as the solute, and the other atoms as the solvent. Using definitions (2.7-8) and equation (2.2), the solute probability function for each ordered phase is Fourier transformed. The resulting ordering wave amplitudes for the ordered rhombohedral phases are given in table 2.

In describing these phases it is useful to make use of the concept of an ordering star. The star of k is the set of non-equivalent wave vectors obtained by applying the point operations of the fundamental lattice onto the wave vector k.

Two wave vector k and k' are equivalent if they differ by an reciprocal lattice vector, i.e., $k - k' = H$ where H is a reciprocal lattice vector. This definition follows from equation (2.6). Since the wave function $p_k(r)$ is evaluated over the discrete sites of the fundamental lattice, $p_k(r) = p_{k'}(r)$ if k and k' are equivalent wave vectors.

Let us consider the calcite sample. Within the calcite matrix, α (FCC), the two ordered precipitate phases are observed are ν $(AuCu)$ and μ (Cu_3Au). The $AuCu$ phase is generated by the ordering wave $(0,0,1)$, whereas the Cu_3Au phase results from a superposition of the three ordering vectors in the star of $(1,0,0)$, i.e., $(1,0,0)$, $(0,1,0)$, and $(0,0,1)$. However, it should be noted that both the $AuCu$ and Cu_3Au phases have ordering wave vectors from the ordering star, $\{1,0,0\}$.

A different set of phases are observed in dolomite. Within the dolomite matrix, β $(CuPt)$, two ordered precipitates phases are observed, γ $(CuPt_3)$ and δ (A_2B). The $CuPt$ phase is generated by the ordering wave $(\frac{1}{2},\frac{1}{2},\frac{1}{2})$, whereas the $CuPt_3$ phase result from a superposition of the ordering waves $(0,0,1)$, $(\frac{1}{2},\frac{1}{2},\frac{1}{2})$, and $(\frac{1}{2},\frac{1}{2},-\frac{1}{2})$. The A_2B phase is a superposition of ordering waves $(\frac{1}{2},\frac{1}{2},\frac{1}{2})$, $\pm(\frac{1}{3},\frac{1}{3},\frac{1}{3})$, and $\pm(\frac{1}{6},\frac{1}{6},\frac{1}{6})$. A feature that these ordered phases in common is that their largest ordering amplitude is at $(\frac{1}{2},\frac{1}{2},\frac{1}{2})$.

C. Equilibrium Conditions

Let the interaction potential be given by the function $V(r)$. The potential $V(r)$ is due to the chemical mixing of ordering species, i.e., $V(r) = V_{AA}(r) + V_{BB}(r) - 2V_{AB}(r)$ where r is the distance between two ordering sites. The configurational energy is

$$E = \frac{1}{2}\sum_{r_1 r_2} p(r_1)V(r_1 - r_2)p(r_2). \tag{2.9}$$

Using equations (2.2) to Fourier transform equation (2.9), one obtains

$$E = \frac{N}{2}\sum_{k} V(k)|Q(k)|^2 \tag{2.10}$$

where

$$V(k) = \sum_{r} V(r)\, e^{-i2\pi k\cdot r} \tag{2.11}$$

and N is the number of atoms.

Using equation (2.10) and the ordering amplitudes given in table 2, the configurational energies for the ordered phases are

$$E_\alpha = 0, \tag{2.12a}$$

$$E_\beta = \frac{N}{2}[\frac{1}{4}V(0,0,0) + \frac{1}{4}V(\frac{1}{2},\frac{1}{2},\frac{1}{2})], \tag{2.12b}$$

$$E_\nu = \frac{N}{2}[\frac{1}{4}V(0,0,0) + \frac{1}{4}V(1,0,0], \tag{2.12c}$$

$$E_\gamma = \frac{N}{2}[\frac{9}{16}V(0,0,0) + \frac{1}{16}V(1,0,0] + \frac{2}{16}V(\frac{1}{2},\frac{1}{2},\frac{1}{2}), \tag{2.12d}$$

$$E_\mu = \frac{N}{2}[\frac{9}{16}V(0,0,0) + \frac{3}{16}V(1,0,0)], \tag{2.12e}$$

$$E_\gamma = \frac{N}{2}[\frac{4}{9}V(0,0,0) + \frac{1}{9}V(\frac{1}{2},\frac{1}{2},\frac{1}{2})] + \frac{1}{18}V(\frac{1}{3},\frac{1}{3},\frac{1}{3}) + \frac{1}{18}V(\frac{1}{6},\frac{1}{6},\frac{1}{6})]. \tag{2.12f}$$

The derivation of equations (4.12a-f) makes use of the fact that the value of $V(k)$ is the same for wave vectors in the same star of k. For example, for the stars $\{1,0,0\}$ and $\{\frac{1}{2},\frac{1}{2},\frac{1}{2}\}$, one obtains the identities

$$V(1,0,0) = V(0,1,0) = V(0,0,1), \tag{2.13}$$

and

$$V(\frac{1}{2},\frac{1}{2},\frac{1}{2}) = V(-\frac{1}{2},\frac{1}{2},\frac{1}{2}) = V(\frac{1}{2},-\frac{1}{2},\frac{1}{2}) = V(\frac{1}{2},\frac{1}{2},-\frac{1}{2}). \tag{2.14}$$

The stars $\{1,0,0\}$ and $\{\frac{1}{2},\frac{1}{2},\frac{1}{2}\}$ are special point ordering stars since the vectors in these stars at located at special point positions in the reciprocal lattice. At the special points, the k-space gradient of any function of k will vanish as a consequence of symmetry. Therefore, at each special point position in k-space, any function $f(k)$ will have a local maximum, saddle point, or local minimum. For example, at the $(1,0,0)$ special point position in the reciprocal space, a four-fold rotation axis intersects a perpendicular mirror. Therefore, expanding $V(k)$ about $k_0 = (1,0,0)$ to the second order, one obtains

$$V(k) = V(1,0,0) + \frac{1}{2}\left[V''_{xx}\delta k_x{}^2 + V''_{yy}(\delta k_y{}^2 + \delta k_z{}^2)\right] \tag{2.15}$$

where $k = k_0 + \delta k$. If $V''_{xx} > 0$ and $V''_{yy} > 0$, then $V(k)$ will have a local maximum at $(1,0,0)$. If the pair potential function $V(k)$ does not have accidental minima, i.e., minima due to symmetry, then the global minima of $V(k)$ must be at one of the special point positions.

The equilibrium phase is determined by the minimization of the energy. Let us consider the consequences of assuming that the $V(k)$ minima are at

either $\{1,0,0\}$ or $\{\frac{1}{2},\frac{1}{2},\frac{1}{2}\}$. There are two phases with Ca composition 50% - β $(CuPt)$ and ν $(AuCu)$. Likewise, there are two phases with Ca composition 75% - γ $(CuPt_3)$ and μ (Cu_3Au). To determine the conditions for homogenous ordering, the energies of phases with same composition are compared. If the $V(k)$ minima is at $\{1,0,0\}$, then by equations (2.12e-f), the ν and μ phases have the lower energy for compositions 50% and 75%, respectively. These are the ordered precipitates phases observed in calcite. On the other hand, if the $V(k)$ minima is at $\{\frac{1}{2},\frac{1}{2},\frac{1}{2}\}$, then the β and γ phases have the lower energy for compositions 50% and 75%, respectively. These ordered phases are observed in dolomite.

The occurrence of the δ (A_2B) phase in dolomite is also consistent with the assumption that the $V(k)$ minima is at $\{\frac{1}{2},\frac{1}{2},\frac{1}{2}\}$. This is because the largest (dominant) ordering wave amplitude of the δ phase is at $(\frac{1}{2},\frac{1}{2},\frac{1}{2})$. By Khachaturyan's maximum amplitude principle [9], for a fixed composition, the system seeks to maximize the ordering wave amplitude corresponding to the $V(k)$ minima, but the ground state condition may require the formation of additional ordering waves. His theory predicts that the wave vector of the dominant (largest amplitude) ordering wave(s) correspond to the positions in k-space where $V(k)$ has minima. For the composition (2/3) Ca and $V(k)$ minima at $\{\frac{1}{2},\frac{1}{2},\frac{1}{2}\}$, by Khachaturyan's maximum amplitude principle, the minimum energy homogenous ordering configuration is an ordered sequence on consecutive $< 1,1,1 >$ planes of the pseudocubic FCC ordering frame. The pattern of this sequence is $\ldots(CaMgCaCaCaMg)\ldots$. This is the ordering pattern observed for the δ (A_2B) phase.

From these considerations, it follows that the $V(k)$ minima are at $\{1,0,0\}$ for calcite and at $\{\frac{1}{2},\frac{1}{2},\frac{1}{2}\}$ for dolomite. The difference in the pair potential functions for ordering in calcite and dolomite is likely due to the fact that for the ordered phases in calcite there is a binary ordering of Ca and Mg, whereas for the ordered phases in ferroan dolomite there is a pseudobinary ordering of Ca and Mg_xFe_{1-x}. Hence, the addition of Fe causes the pseudobinary pair potential for dolomite to differ from the binary pair potential for calcite.

An important point to note is that whereas all of the ordered phases observed in calcite require that the $V(k)$ minima be at $\{1,0,0\}$, all of the ordered phases in dolomite require that the $V(k)$ minima be at $\{\frac{1}{2},\frac{1}{2},\frac{1}{2}\}$.

D. Ordering Wave Instabilities

For stability of the disordered state, the second order coefficient $b(k)$ in the free energy expansion

$$F = F^0 + \frac{1}{2}\sum_k b(k)|Q(k)|^2 \tag{2.16}$$

must be positive for all values of k. The coefficient $b(k)$ is composition and temperature dependent, i.e., $b(k) = b(k;c,T)$. If $b(k)$ is negative, then ordering waves with wave vector k will form spontaneously. Khachaturyan has shown that mean-field theory predicts that the ordering wave instability will occur if the temperature is below the instability temperature

$$T^*(k) = -V(k)c(1-c) \tag{2.17}$$

where c is the composition and k is the wave vectors of the instability ordering waves [10]. The highest instability temperature will be for ordering

waves with the most negative value of $V(k)$. Hence, the ordering wave vectors for the ordering wave instability will be the vectors in the star of k corresponding to the $V(k)$ minima. Since the minima are most likely to be at the positions of a special point star, the ordering wave instability is most likely to produce a special point superstructure.

After the initial instability, the state of the system may evolve rapidly if the ordering transition is of the first kind. Hence, during the time between the initial instability and the final formation of the precipitate phase, the system may be in transient states of non-equilibrium. Ordering wave instabilities will occur for all ordering wave vectors for which $b(k;T,c) < 0$. If the temperature is below the instability temperature, $b(k;T,c)$ will be negative for some region surrounding points where $V(k)$ takes on its minimum value. This leads to superposition of ordering waves with wave vectors within the $b(k;T,c) < 0$ region. However, the growth rate of the ordering waves is largest for the wave vectors for which $V(k)$ is the most negative. Hence, the ordering waves corresponding to the $V(k)$ minima will grow fastest. Therefore, the kinetics of the instability transition favors the formations of ordering waves with wave vectors at the $V(k)$ minima positions in k-space.

It has been shown that the conditions for equilibrium imply that the $V(k)$ minima are at $\{1,0,0\}$ in calcite and $\{\frac{1}{2},\frac{1}{2},\frac{1}{2}\}$ in dolomite. Both $\{1,0,0\}$ and $\{\frac{1}{2},\frac{1}{2},\frac{1}{2}\}$ are special point ordering stars. Therefore, special point ordering wave instabilities may occur in both calcite and dolomite.

The ordering wave vectors of the instability ordering waves is deter-

mined by the k-space positions of the $V(k)$ minima. However, if two ordering wave vectors k and k' appear, then the loss of symmetry caused by these waves may introduce the additional ordering wave $k + k'$. Hence, the initial ordering wave instability may produce ordering waves from both the ordering star corresponding to the $V(k)$ minima and additional ordering stars.

Let us consider the possible ordering wave instability in calcite. The transition from the disordered solid solution to ν $(CuAu)$ or μ may occur by means of an $\{1,0,0\}$ ordering wave instability. While both phases result from the same ordering wave instability, they obtain different crystal structures because $CuAu$ contains only one ordering wave from the $\{1,0,0\}$ star, whereas Cu_3Au contains three ordering waves vectors from the same star.

For the ordering transition in dolomite, the situation is somewhat more complicated. The transitions from the disordered solid solution to β $(CuPt)$, γ $(CuPt_3)$, and δ (A_2B) all involve the formation of a $(\frac{1}{2},\frac{1}{2},\frac{1}{2})$ ordering wave. However, the nature of the transitions are different. The transition to $CuPt$ may occur by means of single $\{\frac{1}{2},\frac{1}{2},\frac{1}{2}\}$ ordering wave, whereas for the transition to $CuPt_3$ the initial $\{\frac{1}{2},\frac{1}{2},\frac{1}{2}\}$ instability produces the ordering wave vectors $(\frac{1}{2},\frac{1}{2},\frac{1}{2})$ and $(\frac{1}{2},\frac{1}{2},-\frac{1}{2})$, but the symmetry breaking of these waves leads to the simultaneous formation of a $(0,0,1)$ ordering wave vector since

$$(\frac{1}{2},\frac{1}{2},\frac{1}{2})+(\frac{1}{2},\frac{1}{2},-\frac{1}{2})=(1,1,0)\equiv(0,0,1) \tag{4.13}$$

The transition to the A_2B phase begins with an initial $\{\frac{1}{2},\frac{1}{2},\frac{1}{2}\}$ instability which produces a non-stoichiometric $CuPt$ phase. The ordering pattern

is $\ldots(CaXCaXCaX)\ldots$ where $X = Ca_x(Mg,Fe)_{1-x}$. This phase can transform to the A_2B phase by replacing the second X in the sequence with Ca, i.e.,

$$\ldots(CaXCaXCaX)\ldots \quad \rightarrow \quad \ldots(CaXCaCaCaX)\ldots. \tag{4.14}$$

This secondary ordering transformation introduces ordering waves from the stars $\{\frac{1}{3},\frac{1}{3},\frac{1}{3}\}$ and $\{\frac{1}{6},\frac{1}{6},\frac{1}{6}\}$. However, if the $V(k)$ minima are at $\{\frac{1}{2},\frac{1}{2},\frac{1}{2}\}$, the $(\frac{1}{2},\frac{1}{2},\frac{1}{2})$ ordering wave should form first by instability. The additional ordering waves then form as the temperature is lowered sufficiently below the instability temperature. This is because at Ca composition (2/3), a single $(\frac{1}{2},\frac{1}{2},\frac{1}{2})$ ordering wave cannot exist in the ground state.

III. DISCUSSION AND CONCLUSION

Compared to metals, minerals are much more complicated in structure. Yet, it has been shown that the cation ordering in the rhombohedral carbonates can be theoretically investigated by analogy with FCC based metal alloys. I will now discuss how this analogy provides a simple means of explaining how the precipitates in calcite and dolomite may have formed.

If a metal alloy is heated to a sufficiently high temperature, its atoms will disorder over the sites of the ordering frame. To discuss the sequence of events that occur upon cooling of the alloy there are two temperatures of interest. One is the transition temperature T^0 and the other is the instability temperature T^*. If the alloy is cooled to a temperature between T^0 and T^*, then there is a thermodynamic driving force for the disorder to ordering transformation, but the disordered alloy is still thermodynamically stable.

Hence, the transformation requires nucleation and growth. However, if the alloy is cooled below the instability temperature, then the disordered alloy becomes thermodynamically unstable. This may lead to the spontaneous formation of ordering waves. Initially, the amplitudes of these waves are small, but they grow with time and eventually produce ordered phases.

The calcite and dolomite minerals are believed to have grown out of an aqueous solution at a temperature well below the cation ordering temperature. In this case, the initial disordering of cations could not have been produced by thermal forces. However, as the metals and carbonate ions are transferred from the aqueous solution to the surface of the mineral, it seems likely that the initial surface configuration of the cations will be random. That is, while the cation and anions position themselves according to the crystal pattern of calcite, the metal ions are randomly distributed over the cation sites. Since the cation sites form a FCC array, the subsequent cation ordering may be discussed by analogy with FCC based alloys.

At the temperature where the calcite and dolomite minerals form, the kinetics in the bulk are too slow for cation ordering. However, near the surface where the cations and anions are more loosely bound, the kinetics of cation ordering may be sufficiently rapid to permit the formation of precipitates. After these precipitates form, the crystal continues to grow, thus enclosing the precipitates in the bulk. Once inside the bulk, the kinetics are too slow for the precipitates to dissolve. Hence, the precipitates that initially formed near the surface become trapped within the bulk.

Let us now discuss the cation ordering using the theoretical results of

the last section which was based on the assumption that the cations ordered over the sites of a pseudocubic FCC array. The ordering of cations over the sites of the FCC fundamental lattice can then be described using the ordering wave representation. It has been shown that the ordered phases in calcite are generated by ordering waves from the $\{1,0,0\}$ star. The ordered phase in dolomite is more complicated, but the dominant (largest amplitude) ordering wave is from the $\{\frac{1}{2},\frac{1}{2},\frac{1}{2}\}$ star. The stars $\{1,0,0\}$ and $\{\frac{1}{2},\frac{1}{2},\frac{1}{2}\}$ are located at the special point positions in the reciprocal space of the FCC fundamental lattice. The special point positions are significant in that the minima and maxima of any function of wave vector is most likely to fall at these points.

Let $r(k)$ be the rate of formation of ordering waves with wave vector k. This may be defined by the rate of change of the ordering wave amplitude $Q(k)$, i.e., $r(k) = \frac{\partial|Q(k)|}{\partial t}$. The most likely maxima positions of the function $r(k)$ are at the special point positions. This can be explained in the following way. Let us assume that the ordering energy results from pairwise interactions. Then the energy of an ordering wave with amplitude $Q(k)$ is $V(k)|Q(k)|^2$. This implies that the change of energy due to a change in wave amplitude is linearly proportional to $V(k)$. The most likely change in state are those which produce the most negative change of energy. Thus, as $V(k)$ becomes more negative, $r(k)$ increases. Therefore, the maximum rate $r(k)$ will be for the wave vectors corresponding to the $V(k)$ minima. Hence, by this logic, the formation of special point ordering waves is a consequence of $V(k)$ having minima at special point positions.

It follows from these considerations that the observed cation ordering

can be explained solely in terms of kinetics. However, the results of the previous section show that the cation ordering can also be explained in terms of thermal forces. It was shown that if the ordered phases are predicted by minimizing the homogenous ordering energy, then it follows that the observed ordered structures in calcite and dolomite are consistent with the assumption that the $V(k)$ minima are at $\{1,0,0\}$ and $\{\frac{1}{2},\frac{1}{2},\frac{1}{2}\}$, respectively. This result was achieved by a consideration of the conditions for ground state equilibrium and ordering wave instabilities. Below a certain temperature T^* which was called the ordering wave instability temperature, an infinitesimal variation in the ordering wave amplitude $Q(k)$ will lower the mean-field free energy if the temperature is below $T^* = -V(k)c(1-c)$, where c is the solute concentration. If this condition is satisfied, ordering waves will spontaneously form. Therefore, it follows that a $\{1,0,0\}$ ordering wave instability will occur in calcite and a $\{\frac{1}{2},\frac{1}{2},\frac{1}{2}\}$ ordering wave instability will occur in dolomite. Moreover, it was shown that the ordered phases observed in calcite, ν and μ, can exist as equilibrium phases if the $V(k)$ minima are at $\{1,0,0\}$, whereas the ordered phases observed in dolomite, β, γ, and δ, can exist as equilibrium phases if the $V(k)$ minima are at $\{\frac{1}{2},\frac{1}{2},\frac{1}{2}\}$. However, because more than one type of precipitate is observed within the matrix, the mixture of phases in calcite and dolomite cannot correspond to an equilibrium microstructure. Rather, the system must be metastable. Nevertheless, each precipitate phase should satisfy the conditions for homogenous ordering equilibrium, otherwise an ordering transformation to another phase would likely occur.

From these considerations, it follows that precipitates in calcite and

dolomite can be explained by a kinetic and/or thermodynamic mechanism. The theoretical approach developed in this chapter provides an consistent phenomenological explanation of the experimental observations, however, to establish the theory at a more basic level would require a more detail study such as a first principles calculation or an experimental investigation to determine the sequence of events that produce the precipitates. However, this work suggest that the occurrence of the precipitates in calcite and dolomite may have a rather simple explanation in terms of ordering theory. In particular, the analogy with FCC based ordering provides a means of analyzing the cation ordering by treating it as a specific case of FCC based ordering.

In conclusion, two main results are presented in this chapter. First, it was shown that the observed ordered phases in calcite and dolomite can be described as a distribution of cations over the sites of a pseudocubic FCC array. The ordered phases β, γ, ν and μ were found to be isomorphic with the FCC based special point superstructures $CuPt$, $CuPt_3$, $CuAu(I)$, and Cu_3Au, respectively. Secondly, the occurrence of the observed precipitates can be given a consistent explanation using the pair potential approximation. Of particular importance is the function $V(k)$, which is the Fourier transform of the interaction pair potential $V(r)$. It was shown that the formation of the ordered precipitates could be explained in terms of the k-space positions of the $V(k)$ minima. This result followed from a consideration of kinetic rates for ordering wave growth, thermodynamic ordering wave instabilities, and equilibrium conditions for homogenous ordering. In particular, it was shown that the ordered phases are consistent with a $V(k)$ minima at $\{1,0,0\}$ in calcite and at $\{\frac{1}{2},\frac{1}{2},\frac{1}{2}\}$ in dolomite.

Table 1. Atomic coordinates of cation sites in rhombohedral carbonates and their occupancy [27].

Hexagonal Cell			Pseudocubic Cell			Ca Occupancy					
x	y	z	x	y	z	α	β	ν	γ	μ	δ
0	0	0	0	0	0	1	1	1	1	0	1
1/2	0	0	−1/2	0	1/2	1	1	0	1	1	1
0	1/2	0	1/2	−1/2	0	1	1	1	1	1	1
1/2	1/2	0	0	−1/2	1/2	1	1	0	1	1	1
1/6	1/3	1/6	1/2	0	1/2	1	0	0	0	1	0
2/3	1/3	1/6	0	0	1	1	0	1	1	0	0
1/6	5/6	1/6	1	−1/2	1/2	1	0	0	0	1	0
2/3	5/6	1/6	1/2	−1/2	1	1	0	1	1	1	0
1/3	1/6	1/3	1/2	1/2	1	1	1	1	1	1	1
5/6	1/6	1/3	0	1/2	1 1/2	1	1	0	1	1	1
1/3	2/3	1/3	1	0	1	1	1	1	1	0	1
5/6	2/3	1/3	1/2	0	1 1/2	1	1	0	1	1	1
0	0	1/2	1	1	1	1	0	1	1	0	1
1/2	0	1/2	1/2	1	1 1/2	1	0	0	0	1	1
0	1/2	1/2	1 1/2	1/2	1	1	0	1	1	1	1
1/2	1/2	1/2	1	1/2	1 1/2	1	0	0	0	1	1
1/6	1/3	2/3	1 1/2	1	1 1/2	1	1	0	1	1	1
2/3	1/3	2/3	1	1	2	1	1	1	1	0	1
1/6	5/6	2/3	2	1/2	1 1/2	1	1	0	1	1	1
2/3	5/6	2/3	1 1/2	1/2	2	1	1	1	1	1	1
1/3	1/6	5/6	1 1/2	1 1/2	2	1	0	1	1	1	0
5/6	1/6	5/6	1	1 1/2	2 1/2	1	0	0	0	1	0
1/3	2/3	5/6	2	1	2	1	0	1	1	0	0
5/6	2/3	5/6	1 1/2	1	2 1/2	1	0	0	0	1	0

Table 2. Wave vectors k in cubic coordinates of ordering waves and their amplitudes for superstructures of rhombohedral carbonates [27].

$\mathbf{k}_y^c$	$\mathbf{k}_z^c$	α	β	ν	γ	μ	δ
0	0	1	1/2	1/2	3/4	3/4	2/3
0	0	0	0	0	0	−1/4	0
1	0	0	0	0	0	−1/4	0
0	1	0	0	1/2	1/4	−1/4	0
1/2	1/2	0	1/2	0	1/4	0	1/3
1/2	−1/2	0	0	0	−1/4	0	0
1/6	1/6	0	0	0	0	0	−1/6
−1/6	−1/6	0	0	0	0	0	−1/6
1/3	1/3	0	0	0	0	0	1/6
−1/3	−1/3	0	0	0	0	0	1/6

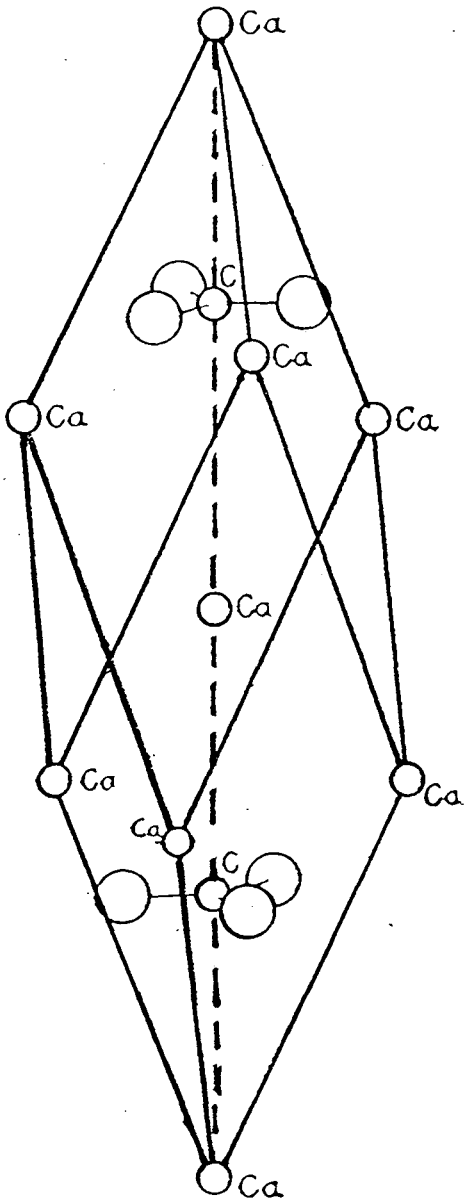

Figure 1. The calcite structure, $CaCO_3$ [32].

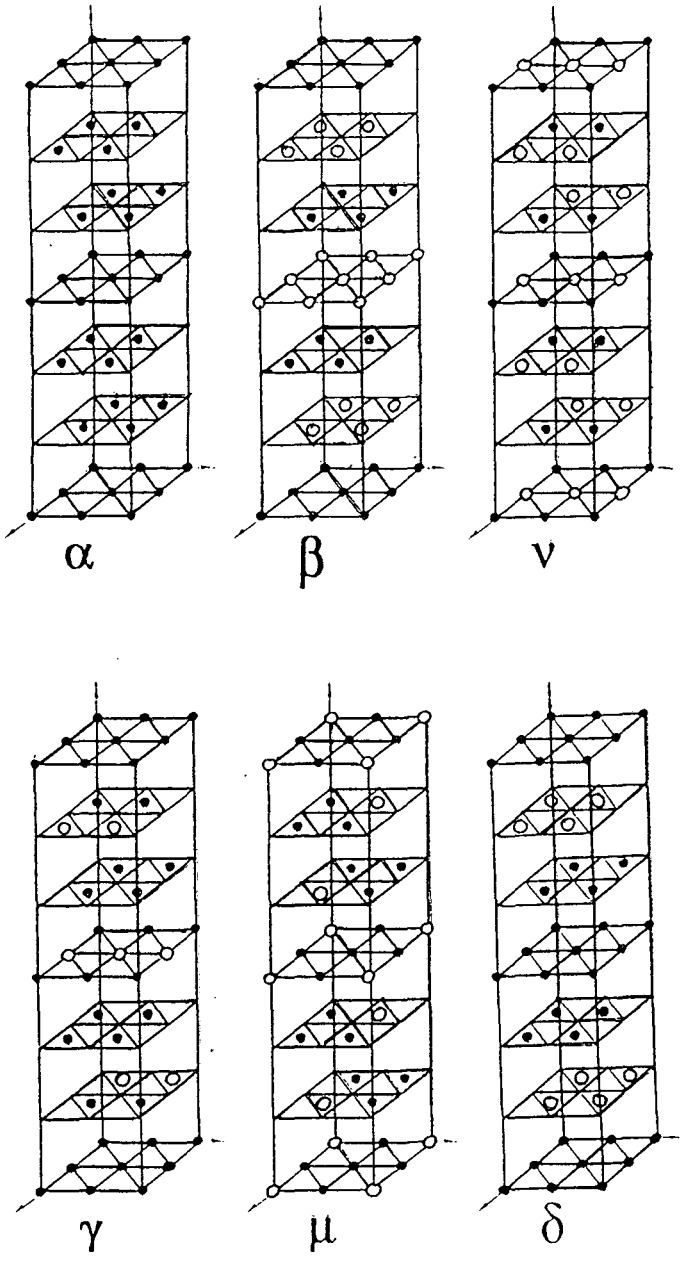

Figure 2. Ordered cation distributions for rhombohedral carbonates in a hexagonal coordinate system [28]. Ca and Mg atoms are represented by closed and open circles respectively. The isomorphic metal phase is given below the greek symbol for each phase.

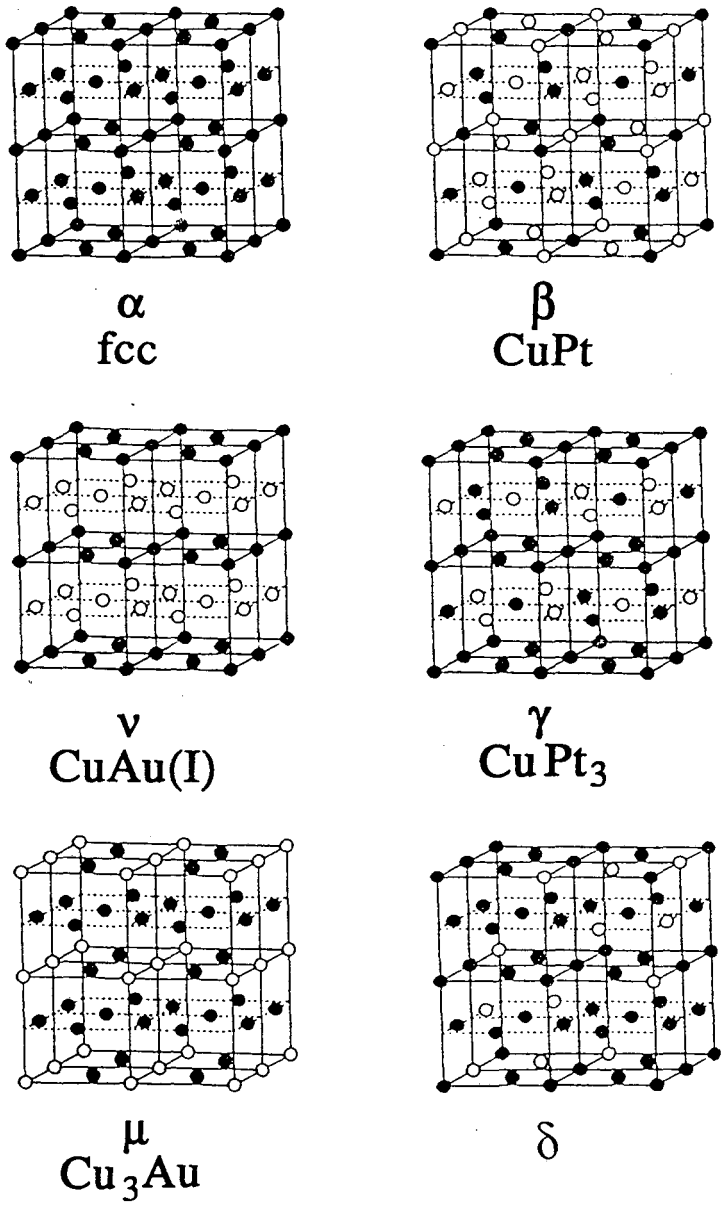

Figure 3. Ordered cation distributions for rhombohedral carbonates in pseudocubic coordinate system [28]. Ca and Mg atoms are represented by closed and open circles respectively. The isomorphic metal phase is given below the greek symbol for each phase.

CHAPTER 4

PRECIPITATION OF $L1_2$ PHASE IN FCC BASED ALLOYS

This chapter presents a theoretical investigation the thermodynamic conditions whereby the $L1_2$ phase may precipitate out of a quenched disordered FCC solid solution. The different transformations paths and mechanism that may the produce precipitates within the matrix are classified. Using a pair potential mean field model, the instability temperatures for spinodal ordering of the disordered phase and spinodal ordering of the homogeneously ordered $L1_2$ phase are computed. This theory is applied to the case of δ' precipitation in the $Al - Li$ alloy. The results predict that depending on which part of the two phase field the alloy is quenched into, the $L1_2$ phase may precipitate out of the disordered matrix, or the matrix may homogeneously order to the $L1_2$ phase which then decomposes to a two phase mixture. Each of these transitions may occur by means of nucleation and growth or by spinodal instability.

I. INTRODUCTION

The $L1_2$ phase is observed as a precipitate phase in many face centered cubic (FCC) based alloys. A two phase mixture of δ' precipitates and α disordered solid solution results from quenching the alloy from above the transition temperature. While the fractions of δ' and α phases are fixed by the conditions for thermodynamic equilibrium, the size and distribution of the δ' precipitates are highly dependent on the transformation path and

mechanism of precipitate formation. In a recent work [29], the thermodynamics of the δ' precipitation was modeled using the pair potential approximation and the mean field approximation. This work predicted that the precipitation process may preceded be preceded by homogenous ordering of the matrix, a result that has been subsequently confirmed experimentally.

In this chapter a theoretical investigation of the transformation paths and thermodynamic mechanisms that produce $L1_2$ precipitates within a disordered matrix is presented. This theory is then applied to the $Al - Li$ alloy system. A good agreement between theory and experimental data is obtained. The context of the problem that will be addressed in this chapter will be discussed to assist in understanding the motivation for this study.

In many metal alloys the atoms are distributed over the sites of an FCC array. The disorder to order transformations produces ordered phases that are superstructures of the FCC structure. One the most common of these is the $L1_2$ structure shown in figure 1. This phase is of significant interest because in many systems it serves as an age hardening precipitate. Since the distribution of precipitates is an important aspect of the microstructure, it is desirable to understand how they form. In many alloys the $L1_2$ type precipitates are known to result from a nucleation and growth process, however, in the $Al - Li$ system, there is experimental evidence that the precipitates result from a spinodal decomposition of a homogeneous ordered $L1_2$ phase .

A nucleation and growth precipitation occurs in the following way. First the alloy is solution treated by heating it to above the transition point.

This produces a disordered FCC solid solution. Then the alloy is quenched to a temperature below the transition point. Assume that the quenched disordered phase is thermodynamically stable, but that it is inside the two phase region of the phase diagram. Thermodynamic fluctuations of the stable phase will cause local variations in the composition. When the local composition is near to the stoichiometric composition of the $L1_2$ phase, an local reconfiguration of the atoms produces a coherently ordered precipitate. The precipitate may subsequently grow thereby decreasing the concentration of the surrounding disordered matrix. This process will continue until the concentrations and fractions of the disordered and precipitate phase have the values required by the phase diagram, that is, until an equilibrium two phase mixture is obtained.

The process of spinodal decomposition for a homogeneously ordered matrix occurs in the following way. Again, the alloy is solution treated by heating it above the transition point. Now assume that upon quenching to alloys transforms homogeneously to the $L1_2$ phase. This ordering transformation can occur by either nucleation and growth, if the temperature is above the supercooling limit, or by ordering wave instability, if the temperature is below the supercooling limit. In either case, one of two possibilities exist. If the ordered phase is stable with respect to composition variations, then the transition to a two phase mixture requires nucleation and growth. However, if not, then a spontaneous variation in the composition will occur. This leads to spinodal decomposition of the $L1_2$ ordered matrix.

The process of spinodal decomposition for a disordered phase is quite

well known. However, the conclusion reached in reference 29 that spinodal decomposition of an ordered phase may also occur is not as well known. Moreover, reference 29 is significant in that it provided convincing theoretical evidence that spinodal ordering of the $L1_2$ ordered matrix in $Al - Li$ may produce the δ' precipitates observed in that system.

The organization of this chapter is as follows. In section II the transformation paths and mechanisms that may produce a two phase mixture (disordered solid solution + $L1_2$ ordered precipitates) are discussed. The purpose of this section is to emphasize the fact that the existence of different types of transformations paths and mechanisms that follow from general principles of thermodynamics and is therefore not a model dependent result. In section III a thermodynamic analysis using pair potential mean field theory is presented. The analysis is general in that the results apply to all systems where $L1_2$ ordering occurs. In section IV, the results of section III are applied to the $Al - Li$ system and the predicted behavior is discussed. Section V contains a brief summary and discussion of the theoretical results presented in this chapter.

II. TRANSFORMATION PATHS AND MECHANISMS

Suppose that that an initially disordered state α_0 transforms upon quenching to the two phase mixture $\alpha + \delta'$. There are two possible transformation paths. 1) The δ' precipitates grow out of the disordered matrix,

$$\alpha_0 \rightarrow \alpha + \delta. \tag{2.1}$$

2) The matrix homogeneously ordered to a non-stoichiometric $L1_2$ phase δ'_0

which subsequently decomposes to the two phase mixture,

$$\alpha_0 \rightarrow \delta_0' \rightarrow \alpha + \delta'. \tag{2.2}$$

Each transformation can occur by one of two mechanisms: 1) Nucleation and growth, and 2) Thermodynamic instability. This implies that there are six possible methods. The conditions for these methods can be stated using the general principles of thermodynamic equilibrium stability.

A phase is stable if all possible infinitesimal perturbations of its state increase its free energy. Two types of instabilities may occur. The first is instability with respect changes in long wave length composition waves. This leads to spinodal decomposition. The second is instability with respect to the formation of an ordered phase, i.e., an ordering instability. (This is also called spinodal ordering.) However, if the alloy is stable, then a change to another state requires a finite free energy fluctuation. This can be achieved only by a nucleation and growth process.

Suppose that the disordered alloy is quenched to a temperature where it is stable with respect to both spinodal decomposition and ordering. Then the transformation to the two phase mixture can occur only by means of nucleation and growth,

$$\alpha_0 \underset{NG}{\rightarrow} \alpha + \delta. \tag{2.3a}$$

On the other hand of the quenched alloy is unstable with respect to compositional variation, then spinodal decomposition occurs,

$$\alpha_0 \underset{SD}{\rightarrow} \alpha + \delta. \tag{2.3b}$$

In this case composition waves emerge. As regions of the alloy develop local compositions near to the stoichiometric composition of δ', precipitates begin to form at these regions. Hence, the sequence is first spinodal decomposition then ordering.

Suppose that the disordered alloy orders homogeneously after being quenched. If the temperature is below the ordering transition point but above the supercooling limit, the disorder to order transformation will require nucleation and growth, whereas as if it is below the supercooling temperature, then spinodal ordering will occur. The matrix is then a homogeneously ordered $L1_2$ phase. Next, two possibilities exist. The transformation to the equilibrium two phase mixture can occur by spinodal decomposition or by nucleation and growth. For the first case the ordered matrix spontaneously develops compositional waves, whereas for the later case disordered regions emerge out of the ordered matrix. It therefore follows that the following four possibilities exist,

$$\alpha_0 \underset{NG}{\rightarrow} \delta_0' \underset{NG}{\rightarrow} \alpha + \delta', \tag{2.3c}$$

$$\alpha_0 \underset{NG}{\rightarrow} \delta_0' \underset{SD}{\rightarrow} \alpha + \delta', \tag{2.3d}$$

$$\alpha_0 \underset{SD}{\rightarrow} \delta_0' \underset{NG}{\rightarrow} \alpha + \delta', \tag{2.3e}$$

$$\alpha_0 \underset{SD}{\rightarrow} \delta_0' \underset{SD}{\rightarrow} \alpha + \delta'. \tag{2.3f}$$

The precipitation methods given in equations (2.3a-f) are very general. The only assumption so far have been that initially disordered alloy transforms to a two phase mixture and that the ordering transformation involve

only $L1_2$ ordering. Hence, the classification of methods is not dependent on any thermodynamic model. However, to demonstrate how the conditions of thermodynamic equilibrium and stability determine which method produces precipitation, it is useful to introduce a specific thermodynamic model. The pair potential approximation will be used in the mean-field limit since this provides a simple means of computing the free energy, and hence predicting the thermodynamic behavior.

III. THERMODYNAMICS

A. Pair Potential Mean-Field Free Energy

The Al and Li atoms are assumed to be distributed over the sites of a FCC array. The thermodynamic state of the alloy is specified by the probability function, $p(r)$ which defines the probability of each site r being occupied by a solute atom. In the mean field limit and assuming pairwise interactions, the energy is

$$E = \frac{1}{2} \sum_{rr'} p(r) V(r - r') p(r) \tag{3.1}$$

where $V(r)$ is the interaction pair potential and the entropy is

$$S = -\sum_{r} \left[p(r) \ln(p(r)) + (1 - p(r)) \ln(1 - p(r)) \right]. \tag{3.2}$$

The mean field free energy is given by the formula

$$F = E - TS \tag{3.3}$$

where E and S are defined by equations (3.1) and (3.2) respectively and the temperature is units of energy.

Fourier transforming the probability function,

$$p(r) = \sum Q(k) e^{i2\pi k \cdot r} \tag{3.4}$$

where

$$r = a(xe_x + ye_y + ze_z), \tag{3.5}$$

$$k = \frac{2\pi}{a}(k_x e_x + k_y e_y + k_z e_z), \tag{3.6}$$

and a is the cell length of the fundamental FCC cell. Using equations (3.1) and (3.4), the energy may be written in the form

$$E = \frac{N}{2} \sum_k V(k) |Q(k)|^2 \tag{3.6a}$$

where N is the number of atoms in the alloy and

$$V(k) = \sum_r V(r)\, e^{i2\pi k \cdot r}. \tag{3.6b}$$

B. Stability of Phases

Consider the change in free energy resulting from a variation of the probability function. Adding to the equilibrium probability function $\bar{p}(r)$ an additional term $\delta p(r)$, the probability function is

$$p(r) = \bar{p}(r) + \delta p(r). \tag{3.7}$$

Since the first variation in free energy will vanish if the phase defined by $p(r)$ is at equilibrium, the change in the free energy $\delta p(r)$ is, to second order,

$$\delta F = \frac{1}{2} \sum_{rr'} A(r, r') \delta p(r) \delta p(r') \tag{3.7}$$

where

$$A(r,r') = \frac{\delta^2 F}{\delta p(r)\delta p(r')} \tag{3.8}$$

Substituting equations (3.1-4) and (3.6) into equation (3.8), one obtains

$$A(r,r') = V(r-r') + \frac{T\delta_{rr'}}{\bar{p}(r)(1-\bar{p}(r))} \tag{3.9}$$

where $\delta_{rr'}$ is the kronecker delta function.

The eigenvalues of $A(r,r')$ are defined by the eigenequation

$$\sum_{r'} A(r,r')\delta p_i(r) = \lambda_i \delta p_i(r) \tag{3.10}$$

The phase will be thermodynamically unstable if one or more eigenvalues are negative. If the ith eigenvalue is negative, there will be a corresponding fluctuation associated with the eigenfunction $\delta p_i(r)$. The eigenvalues are a function of temperature, composition, and equilibrium probability function $p_(r)$. Hence, the conditions for instability are found by solving for the zero eigenvalues, i.e,

$$\lambda_i(T,c) = 0. \tag{3.11}$$

The instability limit is determined by the highest temperature solution of equation (3.12) for a given composition. The locus of points (T,c) obtained in this way defines the instability limit for the phase defined by the equilibrium probability function.

The Fourier transform $A(r,r')$ is

$$A(k,k') = \sum_{r}\sum_{r'} A(r,r')e^{i2\pi(k\cdot r + k'\cdot r')}. \tag{3.12}$$

Since an phase will have a finite number of non-zero Fourier coefficients $Q(k)$, the matrix $A(k,k')$ can be put in block diagonal form. Hence, to determine the conditions for thermodynamic instability, the eigenvalues of each block must be solved for. The matrices $A(r,r')$ and $A(k,k')$ will of course define the same eigenvalues and vectors, however, for the purposes of the chapter, it is more convenient to investigate the conditions for thermodynamic instabilities using the k-space representation of the matrix A.

C. Conditions for Instability of Disordered Phase

The probability function for the disordered phase α is

$$\bar{p}(r) = c. \tag{3.13}$$

where c is the composition of the alloy. Substituting equation (3.13) into equation (3.9), the matrix A is

$$A(r,r') = V(r-r') + \frac{T\delta_{rr'}}{c(1-c)} \tag{3.14}$$

Fourier transforming equation (3.14) gives the result

$$A_{k,k'} = (V(k) + \frac{T}{c(1-c)})\delta_{kk'}. \tag{3.15}$$

Since this matrix is diagonal, its eigenvalues are

$$\lambda_k = V(k) + \frac{T}{c(1-c)}) \tag{3.16}$$

and have corresponding eigenfunctions

$$\delta p_k(r) = e^{i2\pi k\cdot r}. \tag{3.17}$$

The eigenvalue λ_k will vanish when

$$T = T_k^* = -V(k)c(1-c). \tag{3.18}$$

The highest temperature T_k^* for a given composition determines the instability temperature.

The maxima of T_k^* correspond to the minima of $V(k)$. It therefore follows that in the mean-field limit, the instability wave vector is determine by the k-space positions of the minima of $V(k)$. If the minima of $V(k)$ is at $\{0,0,0\}$, the alloy will be unstable with respect to $k = 0$ waves, i.e., composition waves. On the other hand, if the $V(k)$ minima is at the position of the star of k^*, then the alloy will be unstable with respect to the formation of $\{k^*\}$ ordering waves.

Now consider the transformation of the disordered alloy α_o to the two phase mixture $\alpha + \delta'$. $L1_2$ ordering would not occur unless $V(1,0,0) < V(0,0,0)$. This is because if otherwise the $\{1,0,0\}$ ordering waves of the $L1_2$ phase would increase free energy. The instability temperature for $(0,0,0)$ compositional instability must be lower than for the $\{1,0,0\}$ ordering wave instability. Hence, the disordered phase can not undergo spinodal decomposition, but it can experience a $\{1,0,0\}$ ordering wave instability. From equation (3.18), the $\{1,0,0\}$ ordering wave instability temperature is $T^*_{(1,0,0)} = -V(1,0,0)c(1-c)$.

D. Conditions for Instability of $L1_2$ Ordered Phase.

Consider now the case where the equilibrium phase is an ordered phase.

Writing the stability matrix A in the form

$$A(r,r') = V(r-r') + T\alpha(r)\delta_{rr'} \tag{3.19}$$

where

$$\alpha(r) = \frac{1}{p(r)(1-p(r))}, \tag{3.20}$$

Fourier transforming equation (3.19) gives the result

$$A(k,k') = V(k) + T\alpha(k-k')\delta_{kk'}. \tag{3.21}$$

Note that the off-diagonal matrix element $A(k,k')$ is nonvanishing only when $\alpha(k-k')$ is non-zero, i.e, when the difference between the vectors k and k' is one of the wave vectors of the equilibrium ordered phase. This is because the functions $p(r)$ and $\alpha(r)$ have the same crystal symmetry, and thus, their Fourier transforms $p(k)$ and $\alpha(k)$ will have non-vanishing coefficients for the same wave vectors.

The probability function for the $L1_2$ has non-zero Fourier coefficients for fore k vectors,

$$\begin{cases} k_0 = (0,0,0) \\ k_1 = (1,0,0) \\ k_2 = (0,1,0) \\ k_3 = (0,0,1) \end{cases} \tag{3.22}$$

Hence, $p(k)$ and $\alpha(k)$ will have non-vanishing coefficients for only the wave vectors k_0, k_1, k_2, and k_3. Therefore the matrix $A(k,k')$ can be put a block diagonal form where each block is a 4 by 4 matrix. The basis vectors for the blocks are $k+k_0$, $k+k_1$, $k+k_2$, and $k+k_3$. Using the shorthand notation $V(k) = V_k$ and $\alpha_(k) = \alpha_k$, the the corresponding block matrix is

$$\begin{pmatrix} V_k + T\alpha_{k_0} & T\alpha_{k_1} & T\alpha_{k_2} & T\alpha_{k_3} \\ T\alpha_{k_1} & V_{k+k_1} + T\alpha_{k_0} & T\alpha_{k_3} & T\alpha_{k_2} \\ T\alpha_{k_2} & T\alpha_{k_3} & V_{k+k_2} + T\alpha_{k_0} & T\alpha_{k_1} \\ T\alpha_{k_3} & T\alpha_{k_2} & T\alpha_{k_1} & V_{k+k_3} + T\alpha_{k_0} \end{pmatrix} \tag{3.23}$$

where identities

$$k_i \equiv -k_i \quad i = 1, 2, 3 \tag{3.24}$$

and

$$\begin{cases} k_1 - k_2 \equiv k_3 \\ k_2 - k_3 \equiv k_1 \\ k_3 - k_1 \equiv k_2 \end{cases} \tag{3.25}$$

have been used. (Two wave vector k_i and k_j are equivalent, $k_i \equiv k_j$, if they differ by a reciprocal lattice vector.) Let the four eigenvalues be denoted as $\lambda_1(k)$, $\lambda_2(k)$, $\lambda_3(k)$, and $\lambda(k)$. Each eigenvalue is a function of temperature and composition. At a given composition, the instability temperature is determined by the highest temperature for which there exists a vanishing eigenvalue, i.e.,

$$\lambda_i(k; T, c) = 0. \tag{3.26}$$

To solve for the solution of equation (3.26), one may recognize that the cubic symmetry of the $L1_2$ phase implies the identities

$$\alpha_{k_1} = \alpha_{k_2} = \alpha_{k_3} \tag{3.27}$$

Two cases may occur. If the solution of equation (3.6) is for $k = 0$, then there will be an instability which causes a spontaneous variation in the composition and ordering wave amplitudes of the $L1_2$ phase. However, if the solution of equation (3.6) is for $k = 0$, then the instability introduces new ordering waves with wave vectors given by equation (3.22).

For spinodal decomposition of the ordered δ' phase, the solution of equation (3.6) must correspond to the first case, that is, for $k = 0$. Then since the $L1_2$ phase and the FCC fundamental lattice have cubic symmetry,

the block matrix for $k = 0$ takes the form

$$\begin{pmatrix} V_{000} + T\alpha_{000} & T\alpha_{100} & T\alpha_{100} & T\alpha_{100} \\ T\alpha_{100} & V_{100} + T\alpha_{000} & T\alpha_{100} & T\alpha_{100} \\ T\alpha_{100} & T\alpha_{100} & V_{100} + T\alpha_{000} & T\alpha_{100} \\ T\alpha_{100} & T\alpha_{100} & T\alpha_{100} & V_{100} + T\alpha_{000} \end{pmatrix} \tag{3.28}$$

With some algebra, it can be shown that the eigenvalues of this matrix are

$$\lambda_1 = X + Y \tag{3.29a}$$

$$\lambda_2 = X - Y \tag{3.29b}$$

$$\lambda_3 = \lambda_4 = -V_{100} + T\alpha_{000} \tag{3.29c}$$

where

$$X = \frac{V_{000} + V_{100}}{2} - T\alpha_{000} \tag{3.29d}$$

$$Y = \frac{1}{2}\left[(V_{100} - V_{000} + 2T\alpha_{100})^2 + 12(T\alpha_{100})\right]^{1/2}. \tag{3.29e}$$

From these equations, it is apparent that λ_1 is smallest when order parameter is non zero. (If the order parameter were zero, the probability function would correspond to the disordered state.) The spinodal instability occurs when λ_1 vanishes, i.e., $\lambda_1 = 0$. Solving equation (3.29a) for T and taking the positive solution, the instability temperature is found to be

$$T_s = \frac{B + [B^2 - 4C]^{1/2}}{2} \tag{3.30a}$$

where

$$B = \frac{1}{4}[3V_{000} + V_{100}p_2(1 - p_2) + \frac{1}{4}[V_{000} + 3V_{100}]p_1(1 - p_1), \tag{3.30b}$$

$$C = V_{000}V_{100}p_1(1 - p_1)p_2(1 - p_2). \tag{3.30c}$$

and p_1, and p_2 are the solute probabilities on the corner and face sites of the fcc unit cell respectively. In deriving equations (3.30b-c), the relations

$$\alpha_1 = \alpha_{000} + 3\alpha_{100} \tag{3.31a}$$

$$\alpha_2 = \alpha_{000} - \alpha_{100} \tag{3.31b}$$

were used. These were obtained by Fourier transforming the function $\alpha(r)$ and assuming $L1_2$ symmetry.

The eigenvector corresponding to the eigenvalue λ_1 is

$$\phi = \frac{1}{(1+3\gamma^2)^2}\begin{pmatrix}1\\ \gamma\\ \gamma\\ \gamma\end{pmatrix} \tag{3.32}$$

where

$$\gamma = -\left[\frac{\alpha_{000}}{3\alpha_{100}} + \frac{V(0)-\lambda_1}{T\alpha_{100}}\right] \tag{3.33}$$

The eigenvector ϕ can be transformed from the k-space to real space representation by using the Fourier transform equation,

$$\phi(r) = \sum_k \phi(k) e^{i2\pi k\cdot r} \tag{3.34}$$

The function $\gamma(k)$ will have non-zero coefficients for the vectors $(0,0,0)$, $(1,0,0)$, $(0,1,0)$, and $(0,0,1)$. Therefore, the function $\gamma(r)$ will have $L1_2$ symmetry. Evaluating equation (3.34) leads to the result

$$\phi_1 = \phi(0,0,0) = \frac{1}{(1+3\gamma^2)}[1+3\gamma] \tag{3.35a}$$

$$\phi_2 = \phi(1,0,0) = \phi(0,1,0) = \phi(0,0,1) = \frac{1}{(1+3\gamma^2)}[1-\gamma] \tag{3.35b}$$

The quantities ϕ_1 and ϕ_2 give the variations for the corner and face sites of the FCC fundamental cell. When the $L1_2$ phase is almost fully ordered the coefficient γ is close to unity. Then by equation (3.35b), ϕ_2 is approximately zero. Therefore, the decomposition instability is largely confined to the $(0,0,0)$ sites of the FCC cell.

An important point that has been illustrated by the foregoing derivations is that the instability of the $L1_2$ phase leads to the formation of coupled composition and ordering waves. Hence, when the instability limit is reached, both the composition and ordering wave amplitudes spontaneously change together. The relationship between the couple waves is determined by the eigenvectors of the instability matrix A.

E. Calculation of Phase Diagram and Instability Limits

The probability function for the $L1_2$ phase has the form

$$p(r) = \begin{cases} p_1 = c + \frac{3}{4}\eta & \text{corner sites} \\ p_2 = c - \frac{1}{4}\eta & \text{face sites} \end{cases} \tag{3.36}$$

Using equations (3.1-3,6), the mean-field free energy per site is

$$F_N(c,T,\eta) = \frac{1}{2}\cdot\frac{3}{16}V_{100}\eta^2 - T\left(\frac{1}{4}s_0(c+\frac{3}{4}) + \frac{3}{4}s_0(c-\frac{1}{4})\right) \tag{3.37}$$

where

$$s(x) = -(x\ln x + (1-x)\ln(1-x). \tag{3.38}$$

For equilibrium, the first variation with respect to the order parameter η must vanish, i.e.,

$$\frac{\partial F_N}{\partial \eta} = 0. \tag{3.39}$$

Using equations (3.36-2.38), equation (2.35) becomes

$$\frac{T}{V_{100}} = \frac{\eta}{\left(\ln \frac{p_1(1-p_2)}{(1-p_1)p_2}\right)} \tag{3.40}$$

Equation (3.40) gives the temperature for which an $L1_2$ phase with a composition c and order parameter η is an equilibrium phase. Equation (3.40) may be solved for the order parameter for a given composition and temperature, i.e.,

$$\eta = \eta(c, T). \tag{3.41}$$

Using equation (3.41), one obtains the free energy of the equilibrium phase as function of temperature and composition,

$$F_N^e(c, T) = F(c, T, \eta(c, T)). \tag{3.42}$$

From the function $F_N^e(c, T)$ the two phase solubility limits and the spinodal decomposition instability limits may be obtained. The solubility limits are found by using the common tangent rule, i.e.,

$$\left[\frac{\partial F_\alpha}{\partial c}\right]_\alpha = \left[\frac{\partial F_{\delta'}}{\partial c}\right]_{\delta'}] = \frac{F_\alpha - F_{\delta'}}{c_\alpha - c_{\delta'}}. \tag{3.43}$$

For the $L1_2$ δ' phase to be stable, its second variation with respect to variations in the composition must be positive, i.e.,

$$\frac{\partial^2 F_N^e}{\partial \eta^2} > 0. \tag{3.44}$$

On the other hand, when the second derivative is negative, the ordered $L1_2$ phase is unstable with respect to spinodal decomposition. The decomposition instability will cause a variation in the composition and order parameter

as described in the last subsection. This can be understood in the following way. An initial homogeneously ordered $L1_2$ with composition c is unstable and therefore decomposes into regions with compositions $c_+ = c + \Delta c$ and $c_- = c - \Delta c$. This leads to phases with order parameters $\eta_+ = \eta(T, c_+)$ and $\eta_- = \eta(T, c_-)$ respectively. Therefore, since the ordering amplitudes depend on the order parameter, the coupling between the variation in composition and ordering amplitudes is due to the fact the order parameter is a function of composition.

IV. APPLICATION TO δ' PRECIPITATION in $Al - Li$

In this section the theory presented in last section is used to analyze the δ' precipitation observed in the $Al - Li$ system. The basic approach be to determine the values of V_{000} and V_{100} that produce a best fit with experimental data. The data fit is confined to the low temperatures where the mean-field approximation is valid.

In the analysis that is to follow the reduced temperature

$$\tau = \frac{T}{|V_{100}|} \tag{4.1a}$$

is used so that the results obtained in dimensionless form.

The predicted results are computed by means of the following steps which were performed on a digital computer:

1) Equilibrium order parameter $\eta(c, \tau)$.

The order parameter as a function of composition and reduced temper-

ature τ is determined by equation (3.35). This equation is solved by using the Newton-Ransom method to find the zeroes of the function

$$f(\eta) = \tau - \frac{\eta}{\ln\left(\frac{p_1(1-p2)}{(1-p_1)p_2}\right)} \tag{4.1b}$$

where p_1 and p_2 are defined by equation (3.31). The iteration starts with an initial guess corresponding to a maximum value for the order parameter η. At first the iteration value of η decreases monotonically, then cycles back and forth around the solution, and eventually converges. This technique will find the equilibrium order parameter for stable phases. Equation (4.1) also has other solutions, but these correspond to either the disordered state or an unstable equilibrium phase. However, the iteration technique will alway obtain the stable solution.

2) Superheating limit $\tau_+(c)$.

Below a reduced temperature τ_-, the solution converges to a non-zero order parameter. However, above this temperature, the solution converges to zero which corresponds to the disordered state. This is because for $\tau_- > \tau$, the free energy function $F_N(c, T, \eta)$ will have either a global or local minimum for $\eta \neq 0$. On the other hand, for $\tau > \tau_-$, the free energy function has a global minimum at $\eta = 0$ (disorder) but does not have a local minimum for $\eta \neq 0$. Since the ordered phase can exist above τ_-, it follows that τ_- is the superheating limit.

To determine $\tau_-(c)$, $\eta(c, \tau)$ is calculated for reduced temperature increments of $+.001$ and the value of τ is determined for which the solution of the order parameters goes from positive to zero.

3. Transition temperature $\tau_e(c)$.

The transition temperature is defined by the conditions that the free energies of disordered and ordered state are equal, i.e.,

$$F(c, \tau_e, 0) = F(c, \tau_e, \eta(c, \tau_e)). \tag{4.2}$$

The order parameter η is determined by comparing the two free energies for reduced temperature increments of $+.001$.

4) Homogenous ordering instability limit $\tau_-(c)$.

Using equation (3.18), the reduced ordering instability temperature for $\{1, 0, 0\}$ ordering waves is

$$\tau_-(c) = \frac{T}{|V_{100}|} = c(1-c) \tag{4.3}$$

At this temperature $\{1, 0, 0\}$ ordering wave will form spontaneously. Hence, $\tau_-(c)$ is the super cooling limit.

5) Solubility limits $c_\alpha(\tau)$ and $c_{\delta'}(\tau)$.

One standard method to determine the solubility limits is to match chemical potential using equation (3.38). However, at lower temperatures this method has the problem that the derivative $\partial F/\partial c$ varies very rapidly around the solubility limits. Hence, to match chemical potentials requires a very accurate determine of the compositions for the solubility limits. Therefore, an alternate method is used here that is much simpler to implement on the computer. For a given reduced temperature τ, the free energies of

the disordered and ordered phase are computed for composition increments of +.001. For each composition, the phase with the lowest energy is determined. The corresponding free energy is $F(c, \tau)$. A simple method to find the solubility limits is to plot these points on a sheet of paper and then use a ruler to construct the common tangent. This procedure is easily programmed into the computer. The solution is defined by the line which goes through two points with all other points above the line. In this way, the solubility limits c_α and $c_{\delta'}$ are determined to an accuracy of +.001.

6) Spinodal decomposition region of $L1_2$ phase.

In step 5 the free energy of the ordered phase was computed for +.001 increments of the composition. Let i be an index for the composition, i.e., $c_i = i(.001)$. For stability the second variation of the free energy with respect to variations in compositions must be positive, i.e.,

$$F_{i+1} + F_{i-1} - 2F_i > 0 \tag{4.4}$$

where F_i is the free energy for composition c_i. The spinodal decomposition region is defined as the points (τ, c) for which the $L1_2$ phase is unstable with respect to compositional variations. Hence, in this region equation (4.3) will not hold.

To determine the limits for the spinodal decomposition for a given temperature, equation 4.3 is evaluated for each composition $c_i = i(.001)$. The limit is obtained by finding the composition where the second variation test is passed for c_i but not c_{i+1}. This composition will be called c_{sd}. In this way, the spinodal decomposition limit c_{cd} is determine to an accuracy of +.001.

Calculations show that for a given temperature τ the spinodal decomposition is defined by the inequality

$$c_- < c < c_{sd}. \tag{4.5}$$

where c_- is the composition where the $\{1,0,0\}$ ordering instability will occur, i.e., $\tau = \tau(c_-)$, and c_{sd} is the limit described in the last paragraph.

7) Procedure for fitting theoretical phase diagram to experimental phase diagram.

The phase diagram is defined by the solubility limits c_α and $c_{\delta'}$. The reduced phase diagram is computed for different ratios

$$V^* = -V_{000}/V_{100}. \tag{4.6}$$

For example, the results for V^* values 0.0, 1.0, and 2.0 are plotted in figure 2.

For 0.1 increments of V^* between 0.0 and 2.0, the value of V_{100} is chosen to obtain a best fit with the experimental data shown in figure 3. This produces 21 fitted curves. The best fit curve was obtained for $V^* = -1.3$ and $V_{100}/k = -4060\,K$. Hence, the corresponding value of V_{000}/k was $-5070\,K$. The phase diagrams for these values of V_{100} and V_{000} are plotted in figure 4. In the same figure the experimental points are plotted. Note the that the fit with experimental data is quite good.

8) Predicted theoretical results.

Now that V_{000} and V_{100} have been determined from the experimental data, the temperatures for which the spinodal decomposition and ordering instability occur are predicted.

In figure 5, the phase diagram is constructed by plotting c_α and $c_{\delta'}$. In the same plot, the super heating limit $T^+(c) = |V_{100}|\tau_+(c)$ and ordering instability limit $T^-(c) = |V_{100}|\tau_-(c)$ are plotted. These two curves are plotted as dashed lines.

In figure 6, the phase diagram is constructed again but now shows the limits of the spinodal decomposition region defined by equation (4.5), and also the instability temperature.

Let us now interpret these theoretical predictions. If the solution heat treated alloy is quenched into the two phase region, figure 5 shows that there are three cases to consider. 1) To the upper right of the superheating limit (longer length dashed line), the disordered phase is stable and the matrix can not exist as a homogeneously $L1_2$ ordered metastable phase. 2) Between the dashed lines the disordered phase is stable, but the matrix can now exist as equilibrium or metastable $L1_2$ ordered phase. 3) To the lower left of the supercooling limit, which is the $\{1,0,0\}$ ordering wave instability temperature, (shorter length dashed line), the disordered phase is unstable with respect to the formation of $\{1,0,0\}$ ordering waves. Hence, the matrix will spontaneously homogeneously ordered to the $L1_2$ phase.

If the alloy homogeneously transforms to the $L1_2$ phase, then it may be either stable or unstable with respect to variations in its composition. These results together with the conclusions of the previous paragraph imply that there are four different types of precipitation processes for $Al - Li$. The corresponding regions are marked as A, B, C, and D in figure 6. All of these regions are in the two phase field of $Al - Li$. The predicted behavior for each of these regions is as follows:

Region A The homogenous $L1_2$ ordered matrix is stable with respect to variations in the composition; hence, spinodal decomposition of the ordered matrix can not occur.

Region D The ordered $L1_2$ phase can not exist as an equilibrium or metastable precipitate. Thus, decomposition to the two phase mixture can occur only by nucleation and growth. The right hand side of the region has been previously shown to correspond to the superheating limit. In figure 6, it is indicated by a solid line dividing region D from regions B and C.

Regions B and C. A homogenous $L1_2$ ordered matrix is unstable with respect to variations in the composition, therefore, it will spinodal decompose to the equilibrium two phase mixture. The region for which spinodal decomposition of $L1_2$ will occur is indicated as the cross-hatched region in figure 6. However, for the spinodal decomposition to occur, the homogeneously ordered $L1_2$ phase must form. Below the supercooling limit (dashed line) and inside the spinodal decomposition region (cross-hatched) is region C. In this region, spontaneous $L1_2$ ordering is followed by spontaneous de-

composition. On the other hand, in region B, which is above the superheating limit (dashed line) and inside the spinodal decomposition region (cross-hatched), the homogeneously ordered matrix must form by nucleation and growth. Once formed, it may spontaneously decompose by means of spinodal decomposition.

V. DISCUSSION AND CONCLUSIONS

The best known mechanism of precipitation of an ordered phase out of a disordered matrix is the process of nucleation and growth. In this case the precipitate grows out of the surrounding matrix. The characteristic feature of nucleation and growth is the existence of a free energy barrier for precipitate formation. This implies that the precipitation process requires a thermodynamic fluctuation. Hence, upon quenching a disordered solid solution, the precipitates will take some time to nucleate.

In this chapter it has been shown that there also exist alternative processes. The quenched alloy may first homogeneously order. Then the ordered matrix may decompose into a two phase mixture. There are a rich set of possibilities because both the initial ordering and the decomposition may occur by either nucleation and growth or as the result of a thermodynamic instability.

It has been shown that the pair potential mean field theory predicts that the instabilities are of a specific type, namely, either spinodal decomposition or ordering. Since spinodal decomposition may be viewed as a $k = 0$ ordering wave, these two types of instabilities can be regarded as being different cases

of the same phenomena. The prediction that the instability modes produce ordering waves is a result that followed from the pair potential mean field theory. This theoretical approach is quite simple and provides considerable insight. A case could be made for using more accurate statistical mechanical method for computing the energy and perhaps a more realistic energy model, however, the objective here was more qualitative in nature. In particular, the aim was to show that depending on which region of the two phase field the alloy is quenched into, different types of transformations paths and mechanism may occur. Certainly, the general idea that a disordered phase may homogeneously order and then spinodally decompose can be deduced from general principles of thermodynamics, however, the calculated results provide convincing theoretical reason to believe that this transformation does indeed occur in the $Al - Li$ system. Hence, it is concluded here that the pair potential mean field theory provides a sufficiently accurate method of investigating thermodynamic behavior at temperatures well below the transition point.

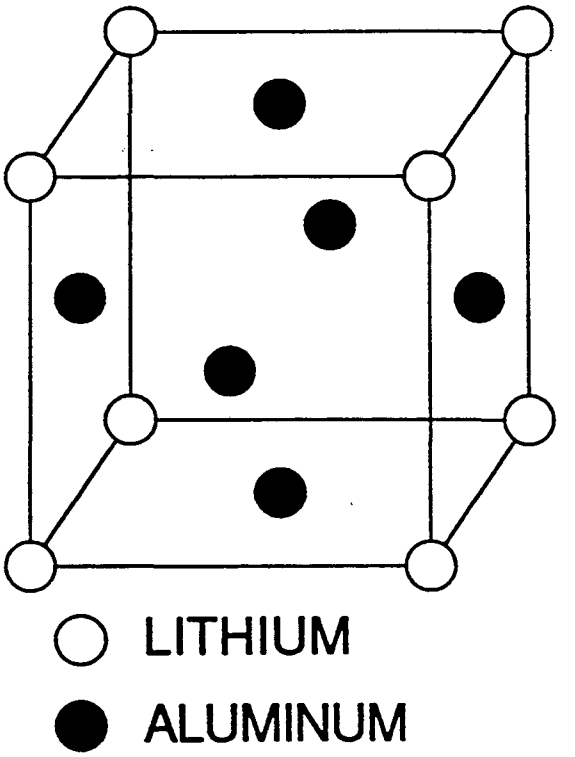

Figure 1. The $L1_2$ ordered superstructure.

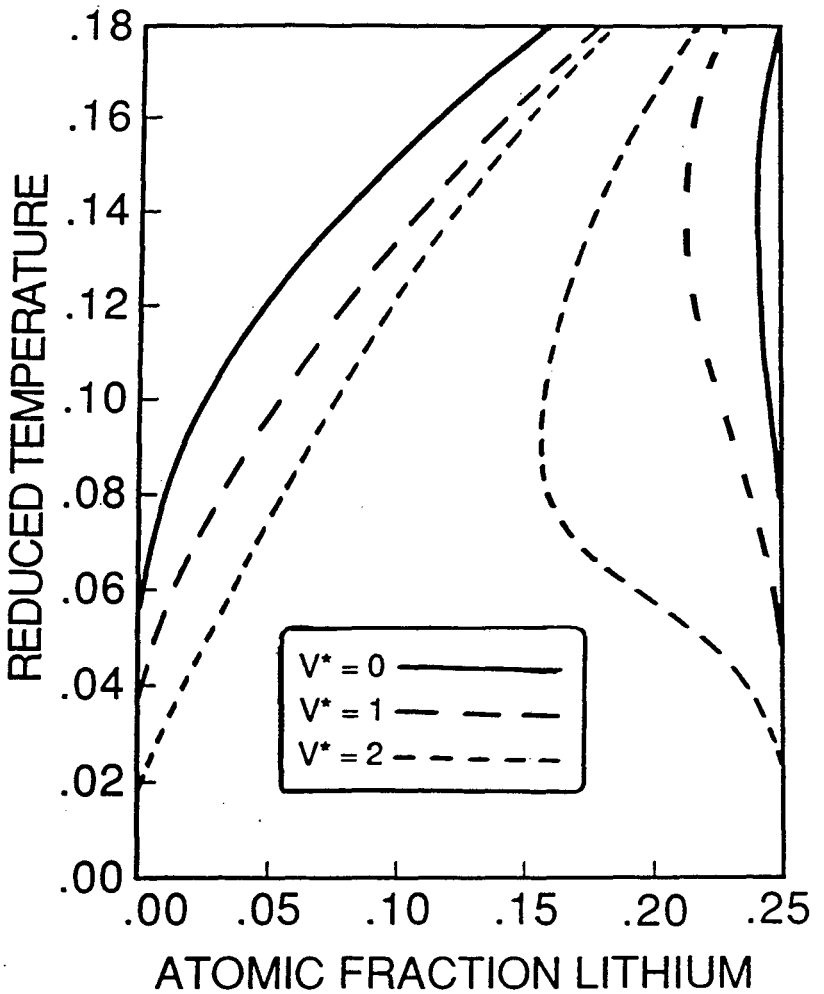

Figure 2. The boundaries of the two-phase region between a disordered solution and an $L1_2$ ordered phase for three values of the interaction parameter, V^* [30].

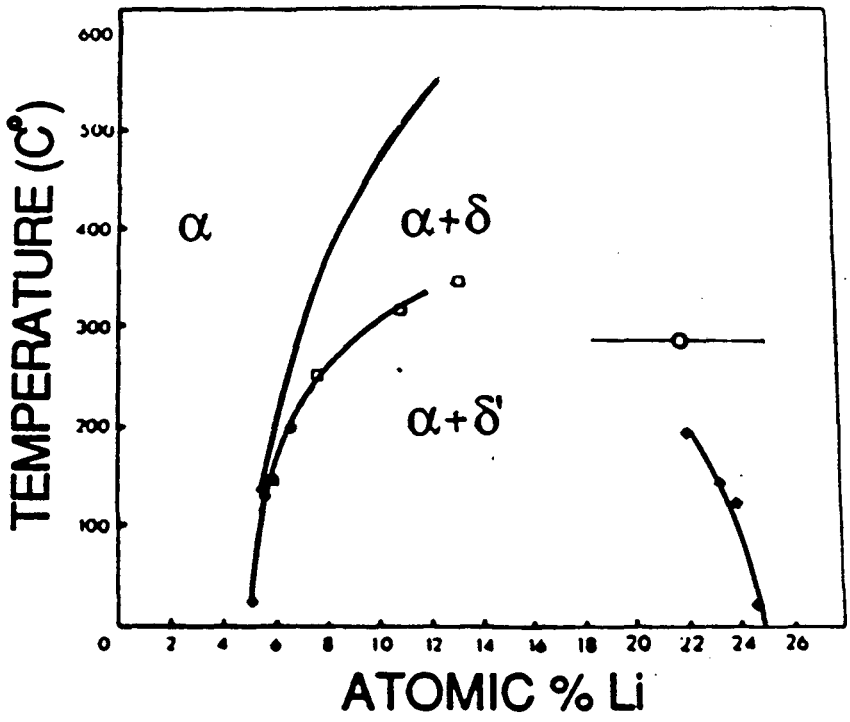

Figure 3. The metastable two-phase region between the disordered $Al - Li$ solution (α) and the Al_3Li phase (δ') in $Al - Li$ [31].

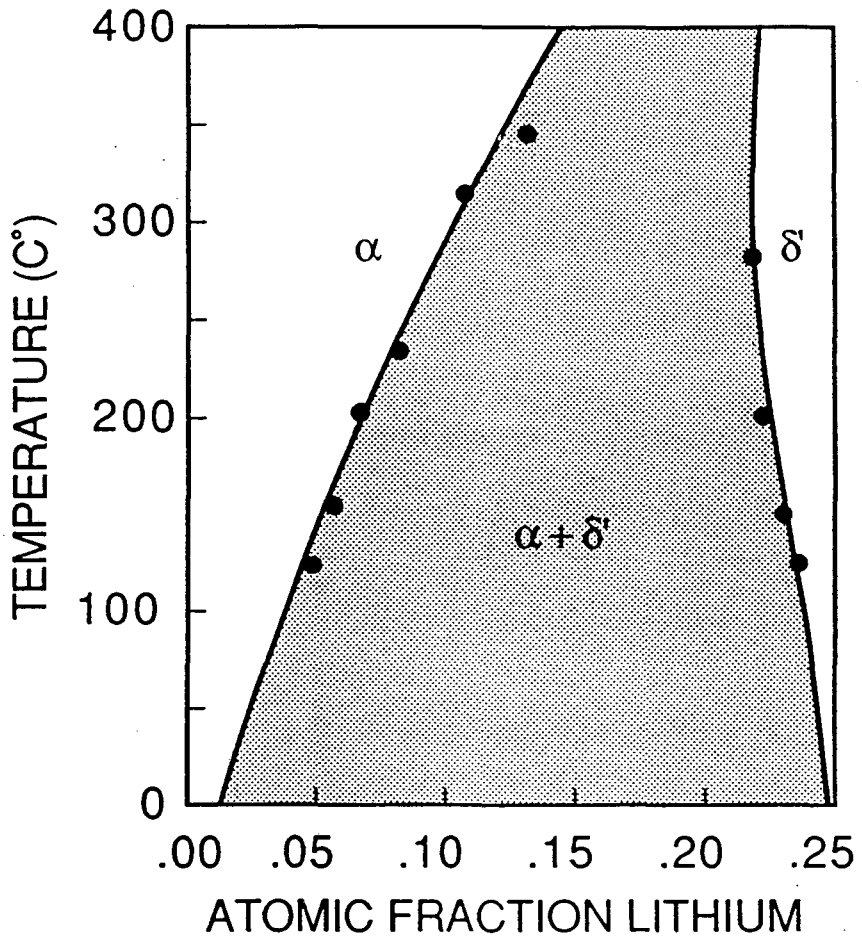

Figure 4. The computed metastable two-phase ($\alpha + \delta'$) region for $Al - Li$ showing the experimental data [30].

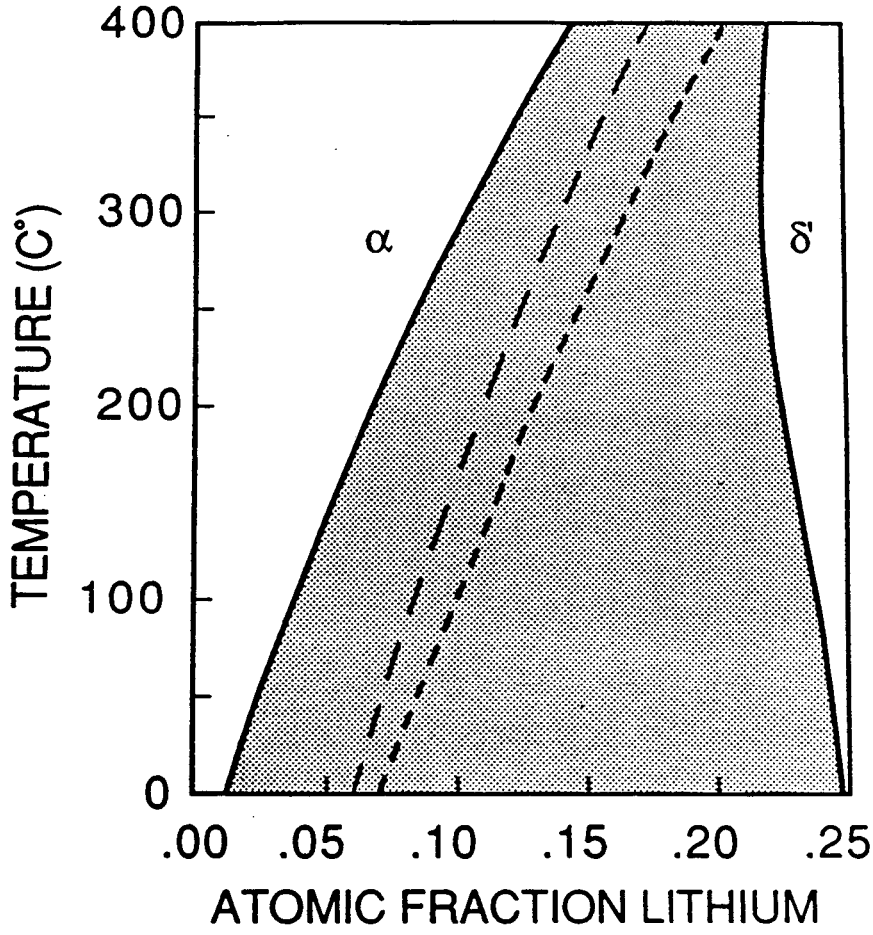

Figure 5. The metastable two-phase ($\alpha + \delta'$) region in $Al - Li$ showing the computed curves for which a disordered solution is metastable with respect to congruent nucleation and growth of the ordered phases (between dashed lines) and unstable with respect to spontaneous, homogenous order (right lower dash line) [30].

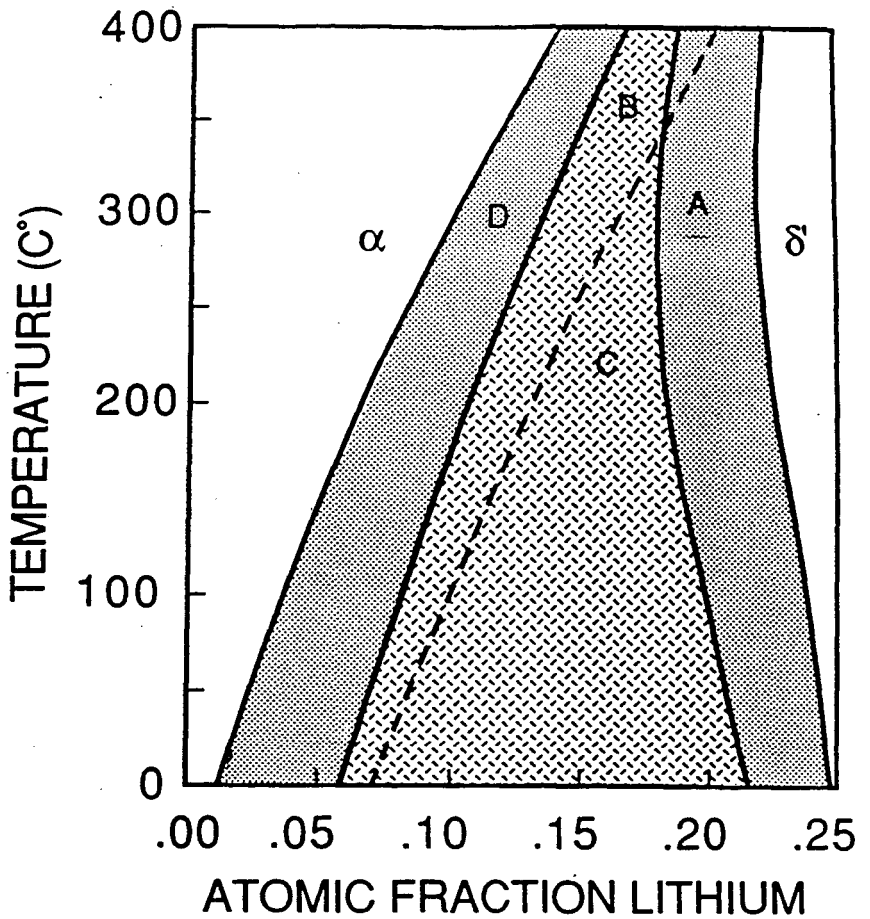

Figure 6. The metastable two-phase ($\alpha + \delta'$) region in $Al - Li$ showing the computed sub-region (lightly shaded) in which a homogeneously ordered Al_3Li phase is unstable with respect to spinodal decomposition. A solution quenched into the regions marked A and D in the figure is metastable. A solution quenched into the region C orders homogeneously (at the dashed line) and then decomposes through a secondary spinodal. A solution quenched into the region B is metastable with respect to order, but will undergo spinodal decomposition if it orders [30].

CHAPTER 5

SUMMARY

A common theme presented throughout this thesis is that both phase equilibria and thermodynamic instability can be explained using the function $V(k)$, which is the Fourier transform of the pair potential function $V(r)$. Since this is a phenomenological quantity, the form of $V(k)$ is deduced from the observed behavior of the system under study.

Chapter 2. Since the ordering amplitudes of the long period superstructures in $Ag - Mg$ and $Al - Ti$ are along the line from $(0,1,0)$ to $(0,1,\frac{1}{2})$ in reciprocal space, the pair potential function $V(k)$ was assumed to have a minimum at some point along that line. To investigate the conditions for which different long period configurations may occur, a Lorentzian form for $V(k)$ was used since it has as the correct general characteristics required for long period ordering. Since it is known that the long period superstructures are very close to being fully ordered, ground state analysis was used. The results show that the dominant wave vectors of the long period superstructure correspond approximately with the $V(k)$ minimum position $(0,1,s/L)$. The integer L determines the crystallographic period, whereas the fraction L/s determines the domain size.

Chapter 3. The ordered precipitates in calcite and dolomite are due to the ordering of cations over the sites of a distorted FCC array. The sites of this array are located interstitially with respect to the carbonate anions. Since the carbonate ions are passive in that they do not take part in the

cation ordering transformation, the cation ordering may be treated as a case of FCC based ordering by ignoring the distortion of the cation ordering array. Ground analysis shows that the dominant wave vectors at are $\{1,0,0\}$ and $\{\frac{1}{2},\frac{1}{2},\frac{1}{2}\}$ for ordered phases observed in calcite and dolomite, respectively. This suggest that the $V(k)$ minima positions for these minerals are at these points in reciprocal space. These points are significant in that they are at special point positions. This is because the most likely positions for the $V(k)$ minima are at these positions. Using mean field theory to determine the conditions for ordering instabilities, the results suggest that a plausible explanation of the observed cation ordering is that an initially disordered cation distribution experiences an ordering instability which produces the ordered precipitates.

Chapter 4. The $L1_2$ precipitate phase is also a special point ordered superstructure. It is generated by a superposition of the special point ordering waves from the star of $\{1,0,0\}$. This suggest that the $V(k)$ minima positions for systems where $L1_2$ phases form are at $\{1,0,0\}$. To investigate the ways in which the $L1_2$ precipitate phase may form, mean field theory was used to analyze the conditions for spinodal ordering and decomposition. The results show that within some portions of the two phase field, (disordered matrix + $L1_2$ ordered precipitates), a quenching of a disordered alloy results in two step precipitation process. The matrix first homogeneously orders to a phase with $L1_2$ symmetry, then this ordered phase spinodally decomposes. The initial homogeneous ordering may occur by nucleation and growth or by spinodal ordering instability.

In this dissertation two major points have be demonstrated. First, the validity and usefulness of using the mean-field and ground state methods at temperatures well below the transition point. (This author certainly recognizes that more precise methods must be used at higher temperatures near the transition point. The point, however, that has been argued is that at sufficiently low temperatures the mean-field and ground state methods are good approximations.) Secondly, the use of the ordering wave method together with reasonable assumptions regarding the locations of the minima of the pair potential function $V(k)$ provides a means of predicting both equilibrium phases and the phase transformation paths.

Long-period ordering, cation ordering in minerals, and precipitation in metal alloys, may seem at first to be very different. However, as shown in this dissertation, these kinds of ordering phenomena may be understood with a common theoretical prospective using mean-field and/or ground state analysis together with the ordering wave representation. Hence, the work presented in this dissertation is an effort toward making the case for the value of using simple methods of analysis that are general enough to be applicable to different types of systems, and thus, hopefully providing a better understanding of how ordering transformations occur.

REFERENCES

1. W.L. Bragg and E.J. Williams, *Proc. Roy. Soc.*, 1934, vol. A145, pp. 699-730.

2. W.L. Bragg and E.J. Williams, *Proc. Roy. Soc.*, 1935, vol. A151, pp. 540-566.

3. E.J. Williams, *Proc. Roy. Soc.*, 1935, vol. 152, pp. 231-252.

4. D. De Fontaine, *Solid State Physics*, 1979, Vol. 34, pp. 73-274.

5. H.A. Bethe, *Proc. Roy. Soc.*, 1935, vol. A150, pp. 552-575.

6. R. Peierls, *Proc. Roy. Soc.*, 1936, vol. A154, pp. 207-222.

7. R. Kikuchi, *Phys. Rev.*, 1951, vol. 81, pp. 988-1003.

8. J. Kirkwood, *Phys. Rev.*, 1938, vol, 6, pp. 38-75.

9. D.A. Badalyan and A.G. Khachaturyan, *Sov. Phys. Solid State*, 1970, vol. 12, pp. 346-351.

10. M.A. Krivoglaz and A.A. Smirnov: The Theory of Order-Disorder in Alloys, American Elveier Pub. Co., New York, NY, 1965.

11. A.G. Khachaturyan, *Prog. Mat. Sci.*, 1978, vol. 22., pp. 1-150.

12. L.D. Landua and E.M. Lifshtiz: Statistical Physics, 3rd ed., Part 1, Pergaman Press, Elmsford, NY, 1980.

13. A. Fisher, Mathematical Theory of Probability, vol. 1, 2nd ed., Macmillian, 1962.

14. P.C. Clapp and S.C. Moss, *Phys. Rev.*, 1968, vol. 171, pp. 754-763; S.C. Moss and P.C. Clapp, *Phys. Rev.*, 1968, vol. 171, pp. 764-777.

15. A.G. Khachaturyan and B.T. Pokrovskii, *Prog. Mat. Sci.*, 1985, vol. 29, pp. 1-135.

16. H. Soto and R.S. Toth, *Phys. Rev.*, 1961, vol. 196, pp.1833-1847.

17. D.A. Vul and M.A. Krivolglaz, 1981, *Phys. Met. Metall.*, vol. 51, pp.1-13.

18. J. Kulik, S. Takeda and D. de Fontaine, 1987, *Acta Metall.*, vol. 35, pp 1137-1147.

19. S. Amelinckx, G. Van Tendeloo, and J. Van Landuyt, 1985, *Ultramicroscopy*, vol. 18., pp. 395-414.

20. K. Schubert, *Trans. JIM*, 1973, vol. 14, pp. 273-280.

21. K. Fujiwara, *J. Phys. Soc. Japan*, 1967, vol. 12, pp. 7-13.

22. M. Tachiki and S. Maekawa, *J. Phys. Soc. Japan*, 1970, vol. 28, pp. 375-379.

23. M. Tachiki and K. Teramoto, *J. Phys. Chem. Solids*, 1970, vol. 28, pp. 335-348.

24. A.G. Khachaturayan, *Prog. Mat. Sci.*, 1985, vol. 29, pp. 1-135.

25. Hansen, Constitition of Binary Alloys, 2nd ed., McGraw-Hill, New York, 1958.

26. H.R. Wenk, H. Meisheng, T.Lindsey, J.W. Morris, Jr., *Phys. Chem. Minerals*,1990, vol. 17, pp527-539.

27. This table has been used in ref. 26.

28. This figure has been used in ref. 26.

29. A.G. Khachaturyan, T.F. Lindsey, J.W. Morris, Met. Trans. A., 1988, vol. 19A, pp. 249-258.

30. This figure has been used in ref. 29.

31. C.M. Sung, H.M. Chan, D.W. Williams, Proc., Third International Conference on Aluminum-Lithium Alloys, C. Baker, P.J. Gregson, S.J. Harris, and C.J. Peels, eds., The Institute of Metals, London, 1986, pp. 337-346.

32. S. L. Bragg, G. F. Claringbull, W. H. Taylor, The Crystalline State, Vol. IV: Crystal Structures of Minerals, ed. S. R. Bragg, Cornell University Press, Ithaca, New York, 1965.

LAWRENCE BERKELEY LABORATORY
CENTER FOR ADVANCED MATERIALS
1 CYCLOTRON ROAD
BERKELEY, CALIFORNIA 94720